

**Estimating the Spatial Distribution of Monthly Mean
Global Solar Radiation Over Ghana Using the
Ångström–Prescott Model**

by

Prince Asilevi Junior, BSc (Physics)

**A Thesis Submitted to the Department of Physics,
Kwame Nkrumah University of Science and Technology
in partial fulfillment of the requirements for the degree**

of

MASTER OF PHILOSOPHY

(Meteorology and Climate Science)

College of Science

Supervisor: Dr. Emmanuel Quansah

©Department of Physics

November, 2016

Dedication

This thesis is dedicated to the

Asilevi family

Abstract

Quantifying the amount of Global Solar Radiation (GSR) reaching the surface of the earth over a specified area is essential for both energy technologies such as solar heating, solar photovoltaics, solar thermal energy, and solar architecture and climate impact studies. In this study, the Ångström–Prescott sunshine duration model is used to estimate monthly mean GSR over Ghana from sunshine duration data measured at twenty synoptic stations distributed across the country. The measured sunshine duration datasets for the model was obtained from the Ghana Meteorological Agency (GMet), distributed over the four agro-ecological zones and spanning a 3-year period (2000 – 2002). The estimated monthly mean GSR datasets were then gridded at a spatial resolution of $10 \text{ km} \times 10 \text{ km}$, establishing the trend and distribution of Global Solar Radiation across the country. The gridded dataset was then compared with satellite data from the National Renewable Energy Laboratory (NREL) and the German Aerospace Centre (DLR) at a spatial resolution of $10 \text{ km} \times 10 \text{ km}$. The results produced appreciable root mean square error values of 1-5, relative mean difference values of 0.03-0.22, absolute mean percent error of 3-29, and correlation coefficient values between 57.8% and 66%. In addition, the estimated total monthly mean Global Solar Radiation over the country is $412.82 \text{ MJm}^{-2}\text{day}^{-1}$ equivalent to 4778.02 Wm^{-2} . The savanna zone has the maximum estimated monthly mean GSR, with the highest level estimated at Navrongo ($20.76 \text{ MJm}^{-2}\text{day}^{-1}$) equivalent to 240.28 Wm^{-2} , showing only 0.32% increment over the study period. The forest zone has the minimum estimated monthly mean GSR, with the lowest radiation level estimated at Oda ($17.11 \text{ MJm}^{-2}\text{day}^{-1}$) equivalent to 198.03 Wm^{-2} . A maximum

and minimum mean clearness index of 0.59 and 0.48 respectively is estimated. This means an estimated 53% of Solar radiation at the top of the atmosphere reaches the study area after attenuation. Meanwhile, the maximum annual time series GSR over the country is within the second trimester of the year (March-April-May), and the minimum annual time series GSR are within the wet and harmattan periods of the year. The satellite data has a total monthly mean Global Solar Radiation of $366.62 \text{ MJm}^{-2}\text{day}^{-1}$ equivalent to 4243.30 Wm^{-2} .

The study shows that solar radiation levels over the country ($17.11 \text{ MJm}^{-2}\text{day}^{-1}$ to $20.76 \text{ MJm}^{-2}\text{day}^{-1}$), meet the international solar technology market standards of $18.7 \text{ MJm}^{-2}\text{day}^{-1}$ to $20.7 \text{ MJm}^{-2}\text{day}^{-1}$ for the operation of photovoltaic systems and solar collectors for industrial and domestic applications.

Contents

Declaration	i
Abstract	iii
List of Figures	viii
List of Tables	xi
List of Symbols	xii
List of Abbreviations	xiii
1 INTRODUCTION	1
1.1 Background	1
1.2 Problem Statement	2
1.3 Justification	3
1.4 Objectives	4
1.5 Thesis Outline	5
2 LITERATURE REVIEW	6
2.1 Solar Radiation: Origin and Physical Nature	6
2.1.1 Origin of Solar Radiation	6
2.1.2 Nature of Solar Radiation	8
2.2 Solar Radiation Data Sources	9
2.2.1 Measurement of Solar Radiation	10
2.2.2 Empirical Models	11
2.2.3 Sunshine duration Models	12

2.3	Solar Radiation and the Atmosphere	15
2.3.1	Solar Atmosphere over Ghana	15
2.3.2	Economic Importance of Solar Radiation	16
2.4	Gridding and Interpolation Techniques	18
2.4.1	Gridding by Minimum Surface Curvature with a Tension Pa- rameter	19
3	RESEARCH METHODOLOGY	21
3.1	Study Area	21
3.2	Methodology	23
3.2.1	Observed Data	23
3.2.2	German Aerospace Centre (DLR) Satellite Data	24
3.3	Model Description and Estimation	25
3.3.1	Angle of Declination	26
3.3.2	Sunset hour Angle	26
3.3.3	Extraterrestrial Solar Flux	27
3.3.4	Clearness Index	28
3.3.5	Length of Day	28
3.3.6	Performance test for Proposed Model Constants	29
3.4	Validation	30
4	RESULTS AND DISCUSSIONS	32
4.1	Clearness Index over Ghana	32
4.2	Estimated Monthly Trend of Global Solar Radiation over the Agro–Ecological Zones	35

4.2.1	The Savanna Zone	35
4.2.2	The Transition Zone	37
4.2.3	The Forest Zone	38
4.2.4	The Coastal Zone	40
4.2.5	Estimated and Satellite Annual Global Solar Radiation	42
4.3	Gridded Estimated Global Solar Radiation	44
4.3.1	Monthly Horizontal Insolation	44
4.3.2	Annual Horizontal Insolation	49
4.3.3	Validation of Estimated Global Solar Radiation	50
4.3.4	Summary of Seasonal and Annual GSR	53
5	CONCLUSIONS AND RECOMMENDATIONS	54
5.1	Conclusions	54
5.2	Recommendations	56
5.2.1	Recommendations for Policy	56
5.2.2	Recommendation for Future Research	56
	Bibliography	57
A	Appendix	67
B	Appendix	71

List of Figures

2.1	Diagrammatic representation of the Earth’s average energy budget. Each number denotes the amount of estimated Global Solar Radiation in Wm^{-2} with their range of uncertainties. They reflect the most accurate predictions for Global Solar Radiation reaching the surface of the earth since the commencement of the twenty first century as presented by Wild et al. (2013)	7
2.2	The spectrum of electromagnetic radiation. Adapted from Duffie and Beckman (1980)	9
3.1	Map of study area (Ghana), showing all twenty-two sites of the Ghana Meteorological Agency (GMET) Synoptic stations recording sunshine duration. The study area is demarcated into four agro–ecological zones, namely Savanna zone, Transition zone, Forest zone, and the Coastal zone. Adapted from Amekudzi et al. (2015)	22
3.2	The Campbell-Stocks sunshine recorder: (a) represents a schematic of the instrument. The part labeled 1 is the glass globe, serving as the concentrating lens, and the part labeled 2 is the concentric mount holding the treated card. (b) represents Photo of a typical Campbell-Stokes sunshine recorder. Adapted from Paulescu et al. (2012) . . .	23
3.3	The rotation of Earth about its axis, showing the angle of declination (δ), and the sunset hour angle (ω)	27

4.1	Clearness Index (CI) over Ghana: (a) represents the monthly mean maximum and minimum CI over the country and (b) represents Clearness Index (CI) for all the four agro-ecological zones.	32
4.2	Estimated Annual Global Solar Radiation Trend for the five sites in the savanna zone of the study area (Wa, Navrongo, Bole, Temale, and Yendi).	35
4.3	Estimated Annual Global Solar Radiation Trends for the three sites in the Transition zone of the study area (Wench, Sunyani, and Kete Krachie). . .	37
4.4	Estimated Annual Global Solar Radiation Trends for the eighth sites in the Forest zone of the study area (Kumasi, Sefwi Bekwai, Oda, Abetifi, Koforidua, Ho, Akuse, Akatsi, Axim, and Takoradi).	38
4.5	Annual Global Solar Radiation Trends for the five sites in the Coastal belt of the study area (Salt Pond, Accra, Tema, and Ada).	40
4.6	Comparing Estimated GSR from the A-P model, and Satellite GSR from the DLR (a) represents the Savana zone, (b) represents the Transition zone, (c) represents the Forest zone, and (d) represents the Coastal zone.	42
4.7	Gridded Monthly Mean Global Solar Irradiance: (a) represents January, (b) represents February, and (c) represents March.	44
4.8	Gridded Monthly Mean Global Solar Irradiance: (a) represents April, (b) represents May, and (c) represents June	46
4.9	Gridded Monthly Mean Global Solar Irradiance: (a) represents July, (b) represents August, and (c) September.	47
4.10	Gridded Monthly Mean Global Solar Irradiance: (a) represents October, (b) represents November, and (c) December.	48

4.11	Gridded Annual mean Global Solar Irradiance.	49
4.12	Gridded Monthly Mean Global Solar Irradiance: (a) represents Estimated GSR for September, (b) represents Satellite GSR for September (c) represents Estimated GSR for October and (d) represents Satellite GSR for October.	50
4.13	Gridded Statistical Tests: (a) represents Root Mean Square Error (RMSE), (b) represents Mean Bias Error (MBE) (c) represents Relative Mean Difference (RMD) and (d) represents Absolute Mean Percentage Error (AMPE).	51
4.14	Gridded Statistical Tests: Left grid represents the Person's Correlation Coefficient; Right grid represents t-statistic test.	52
B.1	Annual Monthly Mean Temperature Trend over the Four Agro-ecological zones of Ghana.	71
B.2	Scatter plots comparing the linear correlation regression between estimated and satellite datasets of Global Solar radiation (GSR) for four selected months over the study area. (a) represents June, (b) represents September, (c) October, and (d) represents November.	72
B.3	Gridded Seasonal Global Solar Radiation estimate: (a) represents December-January-February (DJF), (b) represents represents March-April-May (MAM), (c) represents June-July-August (JJA) and (d) represents September-October-November (SON). The second trimester (MAM) showed the period with the highest Global Solar Radiation ($18.89\text{--}21.74 \text{ MJm}^{-2}\text{day}^{-1}$) levels over the study area, and the third trimester (JJA) showed the period with the lowest levels of Global Solar Radiation ($13.76\text{--}19.81 \text{ MJm}^{-2}\text{day}^{-1}$) for the study area.	73

List of Tables

4.1	Estimated seasonal and annual monthly mean Global Solar radiation for the four agro-ecological zones.	53
A.1	Table showing A-P model constants proposed by Allen et al. (1998) and Anane (1986).	67
A.2	Estimated Monthly mean Clearness Index over the Savanna Zone. . .	67
A.3	Estimated Monthly mean Clearness Index over the Transition Zone. . .	68
A.4	Estimated Monthly mean Clearness Index over the Forest Zone. . .	68
A.5	Estimated Monthly mean Clearness Index over the Coastal Zone. . .	69
A.6	Statistical tests for Model Estimation over Savanna zone.	69
A.7	Statistical tests for Model Estimation over Transition zone.	69
A.8	Statistical tests for Model Estimation over Forest zone.	70
A.9	Statistical tests for Model Estimation over Coastal zone.	70

List of Symbols

T	Temperature	[K]
λ	Wavelength	[m]
ν	Frequency	[Hz]
h	Planck's Constant	[Js]
$\bar{\nu}$	Wave number	[m^{-1}]
δ	Angle of declination	[$^{\circ}$]
ω	Sunset hour angle	[$^{\circ}$]
ϕ	Latitude	[$^{\circ}$]
θ_z	Zenith angle	[$^{\circ}$]
α_s	Solar zenith angle	[$^{\circ}$]
R_o	Extraterrestrial Solar flux	[$MJm^{-2}day^{-1}$]
G_{sc}	Solar constant	[$MJm^{-2}day^{-1}$]
d_r	Earth-Sun distance	[m]
\bar{K}_T	Clearness index	[-]
N	Length of day	[hours]
H	Monthly mean GSR	[$MJm^{-2}day^{-1}$]
P	Rainfall	[mm]
ΔT	Change in Temperature	[K]
K_s	Absorption coefficient	[m^{-1}]

List of Abbreviations

DHI	Diffused horizontal irradiance	[MJm ⁻² day ⁻¹]
DNI	Direct normal irradiance	[MJm ⁻² day ⁻¹]
GSR	Global Solar Radiation	[MJm ⁻² day ⁻¹]
ITCZ	Inter-Tropical Convergence Zone	[-]
SWERA	Solar and Wind Energy Resource Assessment	[-]
DLR	The German Aerospace Centre	[-]
A–P	Ångström–Prescott sunshine model	[-]
TOA	Top of Atmosphere	[-]
GMet	Ghana Meteorological Agency	[-]
NREL	National Renewable Energy Laboratory	[-]
SUNNY	State University of Albany, New York	[-]
RMSE	Root Mean Square Error	[-]
MBE	Mean Bias Error	[-]
RMD	Relative Mean Difference	[-]
AMPE	Absolute Mean Percentage Error	[-]

Acknowledgments

Foremost, I render my sincerest gratitude to the Almighty God, for granting me the opportunity by providence to embark on the ambition of a post-graduate studies. He has been my guide and stay. May His name be praised.

My warmest regards to the supervisor of my research, Dr. Emmanuel Quansah, for his excellent guidance, patience, and providing me with an endearing atmosphere for my research. My skill in working with MatLab, Linux, and Latex were profoundly enhances by his supervision. Dr. Emmanuel Quansah has been supportive since the days I began studying Physics as an undergraduate student.

I would be gravely ungrateful without acknowledging Dr. Leonard Kofitse Amekudzi, who shaped my thinking in Meteorology and Climate Science. Dr. Amekudzi is the “brain” behind my research topic.

A very big thank you also goes to Dr. Michael Edem Donkor. I am exclusively indebted to him for my skill in advanced programming. God richly bless you Doc. I would also want to thank Aryee Jeffrey for his immense contribution to my thesis write-up.

Finally, I would like to thank my mother, Betty Asilevi, Pastor Clifford Assumanihg Marfo, and Asare Kuffour Annabel for always cheering me up and offering me the moral support through the good times and bad.

Chapter 1

INTRODUCTION

1.1 Background

The Sun's energy is the primary source of energy for the earth. This energy called solar radiation or solar irradiance is the driver of all physical, chemical, and biological processes (Gray et al., 2010; Cunningham et al., 2001). It is the energy living organisms on earth need to prepare food for survival, the energy needed to form fossil fuels and renewable biomass from dead organic matter, and the energy that drives abiotic cycles in the atmosphere, hydrosphere, and lithosphere. Solar energy also drives the hydrologic cycle, supplying streams and rivers with running water, which can be employed to generate electricity in hydroelectric power plants. Solar radiation therefore, is an indispensable parameter in the field of architectural design, evapotranspiration estimates for agriculture, and atmospheric, land, ocean, and hydrologic models. Accurate determination of the solar radiation reaching a particular geographical area, and its variations are important because of their potential link with climate variability (Kaufman and Franz, 1996).

The quantity of radiant energy from the sun impinging the ground, is thus needed for application of biophysical and hydrological models to monitor fire outbreaks in forest lands, food production models and other statistical models of environmental phenomena. The efficiency of such models is undoubtedly dependent upon the availability of

measured for solar radiation data (Ramanathan, 1987; Quansah et al., 2014).

The quantity of radiant energy from the sun reaching a particular area at the surface of the earth, can be measured with the pyranometer (Wansah et al., 2014). Provided the measurement instrument can be efficiently maintained, adjusted and examined for faults, and readings regularly taken, ground based recorded data at the meteorological station is the best source of solar radiation data (Bojanowski et al., 2013). Nevertheless, such direct station recorded data are unavailable for most developing countries owing to cost of measurement instrument and lack of technicians to handle the instrument. It is therefore indispensable to investigate methods of estimation from readily available atmospheric data (Tahâş et al., 2011).

1.2 Problem Statement

The ever increasing demand for energy is an inevitable reality, necessary to sustain the economy and to enrich our civilization. The main problem therefore, is to explore alternative sources of energy, especially renewable ones such as solar radiation. Extensive use of fossil fuels and nuclear energy has created deteriorating environmental, social, and sustainable problems. Furthermore, conventional energy systems using fossil resources, especially old ones in numerous and small scale, are found to be major contributors to atmospheric pollution and the greenhouse effect. Renewable sources of energy that will be forever and can be used with minimal pollution, is therefore in global demand (Pandey and Katiyar, 2013)

The most important parameters that are often needed in solar energy technology are,

the average solar radiation and its components (diffuse horizontal irradiance (DHI) and direct normal irradiance (DNI)); measurements of which are not available at every location especially in developing countries due to cost, maintenance and calibration requirements of the measuring equipment (Sarsah and Uba, 2013).

In Ghana, the increasing demand for energy, the power rationing and frequent power outages, is an undoubted incentive to consider harnessing solar energy (Kwakwa, 2014). The motivation for this study therefore is to estimate the quantity and spatial distribution of Global solar radiation reaching the country, for application in the field of solar energy technology and climate impact studies.

1.3 Justification

The world is adopting more stringent strategic policies to increase dependence on renewable and sustainable energy sources paralleled by a reduction of its dependence on fossil fuel resources to power its domestic and industrial needs (Hejase and Assi, 2011).

In places where no data for measured values of solar radiation are available, a common approach has been to determine this parameter by appropriate empirically established physical relationships linking Global Solar Radiation with readily available meteorological data. Statistical correlation studies have demonstrated highly positive relationship between radiant energy from the sun impinging the ground and ambient temperature, relative humidity, precipitation, and sunshine duration (Muzathik et al., 2011). In comparing temperature and sunshine based statistical models for predicting radiant energy from the sun over the Ashanti region of Ghana, Quansah et al. (2014)

accounts that, sunshine duration and temperature are viable variables for model estimations. Such estimations have been carried out for Kumasi and Wa in the Ashanti and Upper West regions respectively. A nationwide estimation will contribute to better understanding the distribution and variability of solar radiation across the country. The Global Solar Radiation potential will be a milestone for designing and predicting the performance of solar energy equipment (Poudyal et al., 2012).

Evidently, the acquisition and development of database for the spatial distribution of solar radiation will facilitate the evaluation of solar energy potential as an input to the country's energy budget and other modeling applications (Quansah et al., 2014).

1.4 Objectives

The main objective of this research work is to estimate monthly mean Global Solar irradiance over Ghana derived from Sunshine hour data. The specific objectives are :

- (i) to estimate the Global Solar irradiation over Ghana using the Angstrom–Prescott model;
- (ii) to grid the estimated dataset on a 10 km × 10 km spatial resolution; and
- (iii) to validate estimated dataset with satellite data from the National Renewable Energy Laboratory (NREL) and The German Aerospace Center (DLR).

1.5 Thesis Outline

The thesis is organised into five chapters. Chapter two has five sections. The origin and physical nature of solar radiation as an electromagnetic energy, is discussed in this section. The second section discusses measurement and source of solar radiation data, with a review on various empirical models proposed for estimation. The third and fourth sections review the solar climate over Ghana and solar radiation as a renewable source of energy, vis-a-vis solar energy technology as a prospective source of electricity for the country's national grid. Finally the gridding method used in the study is presented.

Chapter three discusses more on the study area and methodology of the work. In this chapter, sunshine duration as input data obtained from the Ghana meteorological Agency over a period of 43 years, from 1970 to 2013 at 22 synoptic stations widely distributed over the country is used for the model estimation.

Chapter four discusses the observations and analysis made on the estimated Global Solar radiation for all the 22 synoptic stations used in this study. The analysis is made with respect to the four agro-ecological zones (Northern, Transition, Forest, Coastal) of the country, as used in Amekudzi et al. (2015). Gridding and validation of estimated dataset are presented here.

Chapter five presents the conclusion and recommendations deduced from the discussion made on the results from the previous chapter. The recommendations have greater significance with solar power technology investors.

Chapter 2

LITERATURE REVIEW

2.1 Solar Radiation: Origin and Physical Nature

2.1.1 Origin of Solar Radiation

The sun is the only object in the entire solar system, having the enormous mass needed to create the temperature to sustain and produce radiant energy (Christopher-son, 2014). This energy from the sun impinging a particular point at the surface of the earth is referred to as solar radiation (Arku, 2011). In the core of the sun, hydrogen nuclei are fused to form helium nuclei, a process generating huge amount of energy. This energy is concentrated within the photosphere of the sun, keeping the hot star at about 5800 K in temperature. Emanating from the photosphere, this enormous energy from the sun traveling through space, reaches the earth in the form of short-wave radiant energy (Hewitt and Jackson, 2008). The quantity of radiant energy passing an area per unit time is called the radiant flux, and the radiant flux per unit area is represented by

$$E = \frac{d^2Q}{dA dt} \quad (2.1)$$

where Q represents radiant energy. The irradiance is usually expressed in watts per square meter (Wm^{-2}) (Fleagle and Businger, 1981).

The power of the radiant energy proceeding from the sun is about 3.8×10^{20} MW, equaling 63 MW for every one squared metre area of the surface of the sun. This radiant energy is available concentrically around the sun, radiating outwards in all directions.

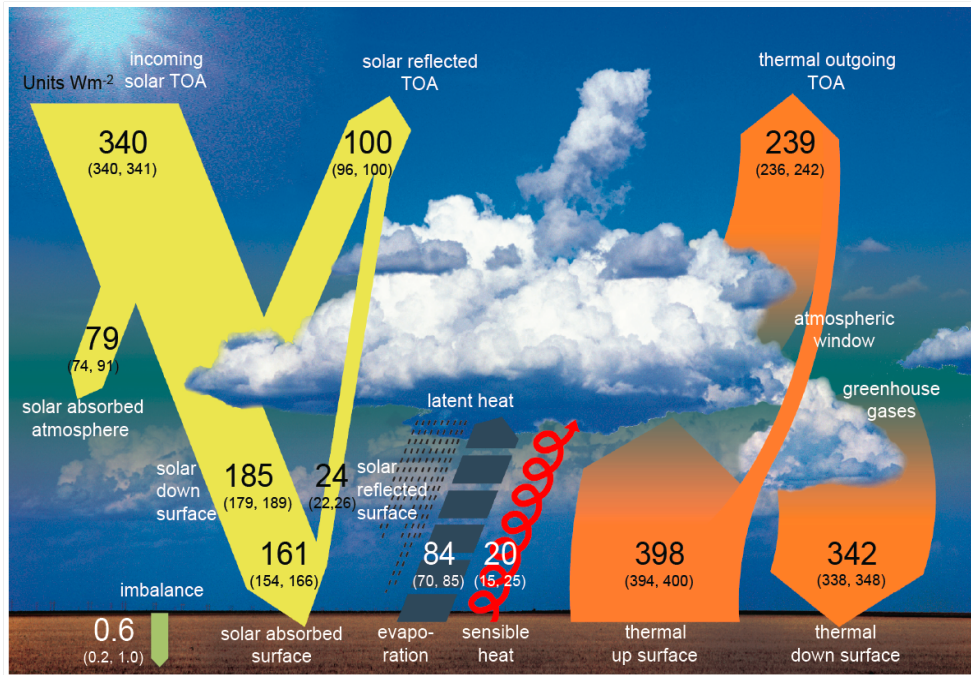


Figure 2.1: Diagrammatic representation of the Earth's average energy budget. Each number denotes the amount of estimated Global Solar Radiation in Wm^{-2} with their range of uncertainties. They reflect the most accurate predictions for Global Solar Radiation reaching the surface of the earth since the commencement of the twenty first century as presented by Wild et al. (2013)

Notwithstanding the fact that only a trivial percentage of this enormous amount of radiant energy proceeding from the sun is interrupted by the earth at a particular point in it's spatial orbit, it is not insignificant. Estimations show that, this trivial percentage supplies radiant energy at the surface of the earth, equivalent to over 10,000 times the current energy demands of the globe (Kalogirou, 2004; Etier et al., 2011).

A recent earth energy budget estimate by Wild et al. (2013), reveals that 22% equivalent to 76 Wm^{-2} of the radiant energy from the sun at the outer "edge" of the

atmosphere suffers backward reflection into space, 23% equivalent to 79 Wm^{-2} is captured by the gaseous envelop of atmosphere through the process of absorption, and 54% equivalent to 185 Wm^{-2} traverses the atmosphere onto the ground (see Figure 2.1).

This amount of surface Solar radiation also called Global Solar irradiance, is affected by the geographical locality, angle of inclination, the hour for the particular day, annual period, and the make-up of the atmosphere at the particular site receiving the radiant energy (Bojanowski et al., 2013).

2.1.2 Nature of Solar Radiation

Radiant energy from the sun impinging the ground is predominantly in the range of visible light, near infrared, and ultraviolet light. According to the principle of the dual nature of light, this incoming radiant energy can be viewed both as a wave and as a stream of energetic particles. Both classifications are significant for engineering applications (Chen, 2011).

(a) The Electromagnetic nature of Solar Radiation

The radiant energy from the Sun is a bundle of varying wavelengths, each bearing peculiar characteristics due to variations in their energies. This bundle of energies is called the electromagnetic spectrum (see Figure 2.2).

Notwithstanding their varying wavelengths and energies, this bundle of radiant energy travels together at the speed of light ($3.0 \times 10^8 \text{ ms}^{-1}$), represented by the expression

$$c = \frac{C_o}{n} \quad (2.2)$$

where C_o (ms^{-1}) is the speed of light in vacuum, and n is the index of refraction for

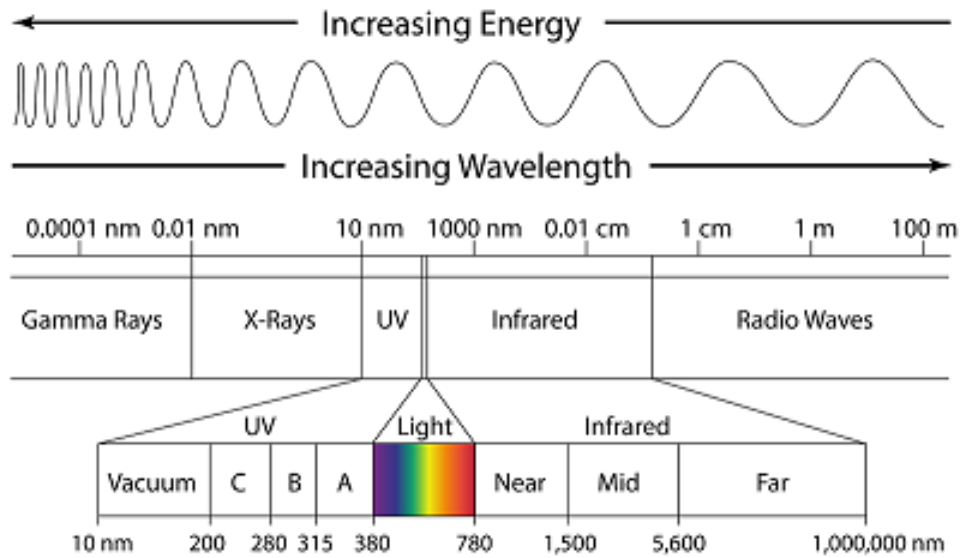


Figure 2.2: The spectrum of electromagnetic radiation. Adapted from Duffie and Beckman (1980)

the medium of propagation (Duffie and Beckman, 1980).

(b) The Photon nature of Solar Radiation

Radiant energy from the sun can also be considered as a stream of energy packets known as photons. By this particulate nature, solar radiation interaction with the atmosphere is the genesis of the earth's climate systems. Measurement of the Global Solar Radiation is thus indispensable, in the pursuit of understanding the weather, global and local climate variability, and the overall energy budget of the earth. It is also required for efficient solar energy technology.

2.2 Solar Radiation Data Sources

In order to successfully design solar technology devices for domestic and industrial purposes, and for a global market to function efficiently, an organised and well documented database for the varying solar radiation across the globe for different sites must be available (Namrata et al., 2012). Currently sources of solar radiation data

include ground based measurements, satellite, and empirical estimations.

2.2.1 Measurement of Solar Radiation

The amount of radiant energy from the sun falling on a horizontal surface (The Global horizontal irradiance (GHI)) reaches the ground in two basic form, namely diffuse horizontal irradiance (DHI) and direct normal irradiance (DNI). The diffused radiation is light which has been scattered before reaching the surface, and the later is light reaching the surface directly from the sun through the atmosphere (Jarraud, 2008). In view of this, two main measurement devices exist to accurately determine the total amount of radiant energy from the sun impinging the ground. Each instrument is designed to capture one form of the impinging radiation. They are the pyrheliometer and the pyranometer.

The pyheliometer detects and measures radiant energy reaching the ground directly from the sun in the form of a beam of light. This measurement device employs the action of a beam collimator. The second instrument namely the pyranometer, measures both beam and scattered light across the dome of the sky. It is capable of detecting the amount of scattered light alone reaching the ground, when obstructed from the direct radiant beam (Duffie and Beckman, 1980).

These instruments for detecting and measuring radiant energy from the sun impinging the ground, are undoubtedly the best. Nevertheless cost of purchase and want of expertise has resulted in limited or in most cases unavailable radiation data for many countries around the globe (Li et al., 2014). Also for the few regions where measurement instruments are mounted, there may occur situations of untrue readings, resulting from instrumental error or sensitivity impairment. These and many

other factors are a great incentive to develop and establish statistical correlation to predict radiant energy from the sun (Gilani et al., 2011).

2.2.2 Empirical Models

Empirical models are statistical correlation equations, which may be linear or quadratic, developed from investigating the regression relationship between solar radiation and other ambient parameter. The correlation equations are based on the presupposition that, the quantity of solar radiation impinging the ground is directly or indirectly proportional to one or more physical variables such as temperature, amount of water vapour in the air, amount of cloud coverage, duration of bright sunshine in hours, and so on (Myers, 2013). The literature stipulates that among the numerous empirical models proposed, the sunshine duration models are the most accurate (Sivamadhavi and Selvaraj, 2012).

Meinel and Meinel (1976), proposed simple correlation equations for predicting direct solar beam from the sun, assuming a cloud and dust free atmosphere. This equation only needed the quantity of radiant energy at the outer edge of the atmosphere, the earth-sun distance factor (R_c), and the optical thickness m (at sea level) of the overlaying atmosphere at the particular site receiving the radiant energy:

$$\text{DNI} = 0.7 R_c I_o^{(0.678m)} \quad (2.3)$$

Laue (1970) further enhanced the model proposed by Meinel and Meinel (1976) to factor the station altitude above sea level. This was an attempt to parameterise the station surface pressure with height (h) as the altitude in kilometres.

Hargreaves and Samani (1982), were the first to propose a model using the difference between the maximum temperature for the day and the minimum temperature for the

night (T_{\max} and T_{\min}) respectively to predict Global solar irradiance as follows:

$$\frac{H}{H_o} = a_1 \Delta T^{0.5} \quad (2.4)$$

where $\Delta T = T_{\max} - T_{\min}$ (K), and a_1 is an empirical coefficient (Li et al., 2014).

Bristow and Campbell, later modified equation 2.4 to capture more site specific details affecting the quantity of incoming radiant energy. Station specific determinants were introduced as shown in equation 2.5, to increase the validity of the equation.

$$H = AH_o[1 - \exp(-B\Delta T^C)] \quad (2.5)$$

where A, B, and C are empirical coefficients unique to each location (Winslow et al., 2001).

2.2.3 Sunshine duration Models

Predicting the quantity of incoming radiant energy from the sun with empirical models from sunshine duration, was first proposed by Ångström (1924). The model was developed from the presupposition that, the degree of clearness of the atmosphere is directly proportional to the cloud index (fraction of possible maximum sunshine). Page (1967) and Prescott (1940) reconsidered this model in order to make it possible to calculate monthly average of the daily global radiation H ($\text{MJm}^{-2}\text{day}^{-1}$) on a horizontal surface from monthly average daily total insolation on an extraterrestrial horizontal surface as per the following relation (Pandey and Katiyar, 2013):

$$\frac{H}{H_o} = a + b \frac{n}{N} \quad (2.6)$$

where H_o ($\text{MJm}^{-2}\text{day}^{-1}$) is the monthly average daily extraterrestrial radiation, n is the monthly average daily bright sunshine hours, N is the maximum possible

monthly average daily sunshine hours or the day length in hours, and a and b are site specific constants. This model has widely been used all around the world, and for selected sites in Ghana (Forson et al., 2004; Anane-Fenin, 1986; Sarsah and Uba, 2013; Quansah et al., 2014).

In the absence of direct measurement of solar radiation to calibrate the Ångström–Prescott sunshine model, Allen et al. (1998) proposed the values of $a = 0.25$ and $b = 0.50$, based on experimental data collected around the world. Anane-Fenin (1986) employed the Ångström–Prescott sunshine hour based model to determine the regression constants ' a ' and ' b ' for the country (Coastal south, Central region, and northern region). These regional constants will be beneficial in estimating Global solar radiation at any site within the country, especially after 1988 when the Bellani Distillation Pyranometers operated by the Ghana Meteorological Agency broke down.

Forson et al. (2004), analysed the annual trend of Global solar radiation at Kumasi, using the sunshine based correlation, and compared the estimated data with ground based measurement from the Solar Energy Applications Laboratory (SEAL) at the Kwame Nkrumah University of Science and Technology (KNUST). The comparison showed very good statistical results. Sarsah and Uba (2013) in a similar analysis, validated estimated solar radiation at Wa in the northern belt, with measured data recorded at Wa Polytechnic. The study further developed multiple linear regression models using three other available meteorological data (ambient temperature, soil temperature, and relative humidity) in addition to the sunshine duration to estimate solar radiation for Wa Polytechnic weather station. The equations developed were a modification of the Ångström–Prescott (A–P) model, with fairly good statistical

test results.

Ogolo (2014), suggested the use of multiple linear regressions that extended beyond the sunshine hour data utilized for the A-P model. In his work, the list of independent variables in the A–P model is enlarged to include temperature, precipitation and relative humidity. The following models were presented:

$$\frac{H}{H_o} = a P + b T + c \frac{n}{N} + d \quad (2.7)$$

where H_o is the monthly average daily extraterrestrial radiation ($MJm^{-2}day^{-1}$), P is the rainfall (mm), T is temperature recorded in degree Celsius, and a, b, c and d are the regression coefficients.

A few contentions however surfaced, with the performance of the above model (Equation 2.7) since rain event is not an all-monthly occurring event, though on annual average, this may be found to be available but relative humidity which is a measure of water vapour in the atmosphere would have been found more suitable. Hence, Equation 2.7 above was modified to replace precipitation with relative humidity.

2.3 Solar Radiation and the Atmosphere

2.3.1 Solar Atmosphere over Ghana

According to Diabate et al. (2004) the solar climate of Ghana is characterised by a maximum atmospheric clearness index in January (0.64), which decreases down to 0.47 in July and increases again over the northern belt, and a maximum atmospheric clearness index from November to May at approximately 0.45, which then decreases to 0.32 in August and then increases again over the southern region. This characterisation coincides with the rainfall and temperature climatology of the country.

The atmosphere of the region is strongly influenced by the West African Monsoon, with rainfall seasons driven by the oscillation of the tropical rain belt, also known as the Inter-Tropical Convergence Zone (ITCZ), which swings back and forth between the northern and southern tropics in each year. The prevailing wind direction in regions south of the ITCZ is southwesterly, blowing moist air from the Atlantic Ocean onto the continent while the prevailing winds to the north of the ITCZ is known as the Harmattan. The Harmattan originates from the northeast, bringing in hot and dust laden air from the Sahara Desert between December and March.

As the ITCZ moves north and south over the year, the zones between the northern and the southernmost positions of the ITCZ experience a shift between the two opposing prevailing wind directions. This pattern is known as the West African Monsoon. The northern part of Ghana experiences a single wet season occurring between May and November of the year when the ITCZ is in its northern position and the prevailing wind is south-westerly. The southern parts of Ghana have two wet seasons: the ma-

major season from March to July, and a minor season from September to November (Nkrumah et al., 2014).

This north-to-south oscillation of the ITCZ eventually controls the dust and moisture compositions (key elements of attenuation of solar radiation) of the atmosphere over the sub-region.

This can be noticed from the clearness index characterisation of the regions atmosphere by Diabate et al. (2004). Clear and dull atmospheres are observed for dry and wet periods respectively. The amount of Global solar irradiance received at the earth surface is thus predominately defined by this regime.

2.3.2 Economic Importance of Solar Radiation

Two indispensable importance of estimated solar radiation can be contemplated. These are solar energy technology and climate variability.

According to the World Energy Council of which Ghana is a committee member, the total world average power at the earth's surface in the form of solar radiation exceeds the total current energy consumption by 15,000 times (Boyle, 1996). The council reported that the world demand for electricity is growing rapidly, and the Primary world energy supply is expected to increase by nearly 60% by 2020. In many developing countries like Rwanda, solar energy technology installations have proven successful (Disch and Bronckaers, 2012).

Agriculture, the main hub of the country's economy and a source of livelihood for the majority of the population, is also heavily dependent on solar radiation. Plants convert the energy from solar radiation into food (chemical energy) by photosynthesis, in the presence of water and minerals from the earth. Furthermore, radiant energy

from the sun traversing the atmosphere, is the principal driver of the weather and local climate. Temperatures at different places vary widely, owing to the fact that surrounding air molecules absorb different amounts of radiant energy and thus are heated at different rates. This creates a temperature gradient, causing winds to blow. Heavy rains characterised by lightening and thunder, are also the results of rapid convective turbulence caused by differential heating in surrounding air. Large quantities of water vapour transported into relatively cooler regions of the atmosphere condenses, producing varied forms of precipitations (Chang, 1974). These and many other atmospheric situations controlled by incoming radiant energy from the sun are indispensable elements of the country's economy.

2.4 Gridding and Interpolation Techniques

The description and distribution of the mean state and variability of recent atmospheric conditions can provide a great deal of information that impacts almost all aspects of human endeavour. Spatio-temporal complete representations of surface climate are required for both applied and theoretical environmental science. Unfortunately most climatological datasets are acquired at widely spaced individual measurement stations, in some cases oblique to each other. This situation of widely spaced recording sites, has created the edge to develop an estimated network of the desired station parameter at some choice resolution from the readily available dataset. This method of creating a fine resolution dataset from a very coarse resolution dataset is called gridding or interpolation (Peterson et al., 1998; Smith and Wessel, 1990). For a sequence of grid points $XYZ \{ (X_i, Y_i, Z_i) \in \mathfrak{R}^3, i = 1, \dots, n \}$, in any 3D space located within a rectangular domain D , an interpolation is produced by solving a continuous function of two independent variables (x,y) , for which $f(X_i, Y_i) = Z_i$. This continuous function is given by:

$$f(x, y) = a.xy + b.x + c.y + d \quad (2.8)$$

where the coefficients a , b , c and d are determined by the corner points of the grid rectangle containing the point (x, y) (Gültekin et al., 2009).

A number of gridding/interpolation methods exist for solving $f(x, y)$. Among these include Triangulation with linear interpolation, Natural neighbour, Inverse distance, Minimum curvature, Regression by plane with weights, Radial basis functions, and Kriging (Smith and Wessel, 1990).

2.4.1 Gridding by Minimum Surface Curvature with a Tension Parameter

This method of gridding and its Computational implementation was first developed by Smith and Wessel (1990). According to this gridding technique, the estimated network dataset created with the Minimum curvature approach is comparable to a flexibly fine flat surface, intercepting all the available site data with very little curves. This computational exercise involves solving the following differentiation equation:

$$(1 - T)\nabla^4 f(x, y) - (T)\nabla^2 f(x, y) = 0 \quad (2.9)$$

The boundaries for the biharmonic differential equation are:

$$(1 - T)\frac{\partial^2 f}{\partial n^2} + (T)\frac{\partial f}{\partial n} = 0 \quad (2.10)$$

and

$$\frac{\partial}{\partial n} (\nabla^2 f) = 0 \quad (2.11)$$

occurring at the sides, at which $\partial/\partial n$ is a differential perpendicular to a particular surface, and

$$\frac{\partial^2 f}{\partial x \partial y} = 0 \quad (2.12)$$

at the corners.

where $T \in (0, 1)$ is a term for the stress within the surface produced, n is the boundary normal, ∇^2 is the Laplacian operator.

$$\nabla^2 = \frac{\partial^2 f}{\partial x^2} + \frac{\partial^2 f}{\partial y^2} \quad (2.13)$$

$\nabla^4 = ((\nabla^2))^2$ is the biharmonic operator.

$$\nabla^4 f = \frac{\partial^4 f}{\partial x^4} + \frac{\partial^4 f}{\partial y^4} + \frac{2\partial^4 f}{\partial x^2 \partial y^2} \quad (2.14)$$

$T = 0$ solves the biharmonic differentiation equation, while $T = 1$ solves the Laplacian differential equation; in this case the resulting surface may have local extremes only at points XYZ.

(Gültekin et al., 2009) has demonstrated that, the minimum surface curvature method of gridding is a viable technique widely used in creating fine resolution network for the spatial variability of ambient temperature, solar radiation, and other Geophysical variables.

Chapter 3

RESEARCH METHODOLOGY

3.1 Study Area

Ghana is the domain of study with four agro-ecological zones adapted from Amekudzi et al. (2015). Dataset from twenty-two different synoptic sites well distributed within these zones were used in the study. From the north the zones are, the Savanna zone with five study sites (Wa, Navrongo, Bole, Temale, and Yendi), the Transition zone with three study sites (Wenchi, Sunyani, and Kete Krachie), the Forest zone with ten study sites (Kumasi, Sefwi Bekwai, Oda, Abetifi, Koforidua, Ho, Akuse, Akatsi, Axim, and Takoradi) and the Coastal zone with four study sites (Saltpond, Accra, Tema, and Ada). Figure 3.1 is a map of the study area, showing the four agro-ecological zones and the twenty two synoptic sites mentioned above.

The Savanna Zone is representative of the southern savanna climatic belt and vegetation, with a mono-modal rainfall pattern, mainly between the months of May and October, while the dry season begins from November and ends in April each year. The dry season is associated with dry and dust-laden ‘Harmattan’ winds with low relative humidity and low night temperatures, while the contrary prevails during the rainy season. The horizontal wind characteristics are predominantly north easterly in the dry season, but south westerly in the rainy season (Quansah et al., 2015).

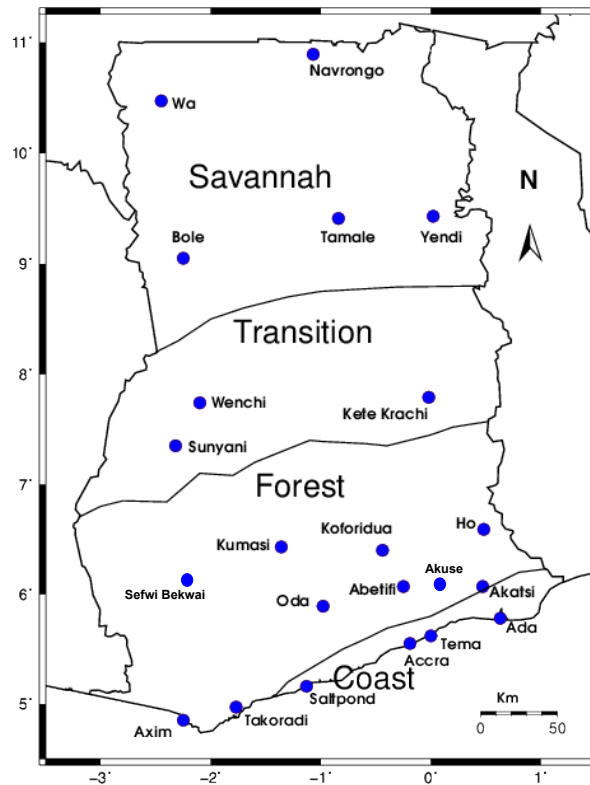


Figure 3.1: Map of study area (Ghana), showing all twenty-two sites of the Ghana Meteorological Agency (GMET) Synoptic stations recording sunshine duration. The study area is demarcated into four agro-ecological zones, namely Savanna zone, Transition zone, Forest zone, and the Coastal zone. Adapted from Amekudzi et al. (2015)

The Transition and Forest zones are the most productive zones of the country in terms of food and cash-crop production, both of which are extremely dependent on traditional rain-fed agriculture. Precipitation records are highest here with an approximate mean annual total of 1800 mm to about 1600 mm (Owusu and Waylen, 2009).

The Coastal zone covers the dry coastal strip of southeastern Ghana, where mean annual rainfalls of between 740 and 890 mm support very little agriculture. The low rainfall is attributed to a complex series of coastal (oceanic) and atmospheric interactions (Owusu and Waylen, 2009).

3.2 Methodology

3.2.1 Observed Data

Sunshine duration datasets for the twenty two synoptic stations distributed over Ghana from 2000 to 2002 were obtained from the Ghana Meteorological Agency (GMet) database. The data was measured with the Campbell-Stokes sunshine recorder, which detects sunshine if the beam of solar energy concentrated by a special lens is able to burn a special dark paper card.

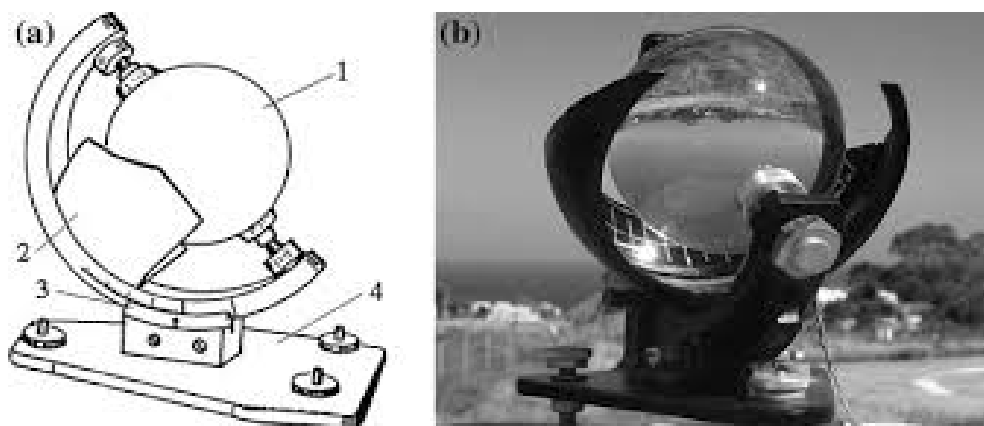


Figure 3.2: The Campbell-Stokes sunshine recorder: (a) represents a schematic of the instrument. The part labeled 1 is the glass globe, serving as the concentrating lens, and the part labeled 2 is the concentric mount holding the treated card. (b) represents Photo of a typical Campbell-Stokes sunshine recorder. Adapted from Paulescu et al. (2012)

The Campbell-Stokes Sunshine recorder is used to measure the actual duration of sunshine, when pyranometers are lacking. In this instrument, a glass globe is used as a lens to concentrate light from the sun onto a card mounted concentrically beneath the glass globe at a certain focal length (see Figure 3.2). According to the World Meteorological Organisation (Jarraud, 2008), sunshine duration during a given period is defined as the sum of that sub-period for which the direct solar irradiance

exceeds 120 Wm^{-2} . As the sun moves over the sky, the position of the focal point changes and a burnt trace is drawn on the card. In the incidence of clouds, the burnt trace is interrupted, owing to reduction in light intensity. The duration of sunshine for a particular day is accounted for by the length of the burnt line segment on the card.

3.2.2 German Aerospace Centre (DLR) Satellite Data

The German Aerospace Centre (DLR) satellite data was prepared for the Solar and Wind Energy Resource Assessment (SWERA) project funded by the United Nations Environment Programme (UNEP) from the Meteosat-7 satellite (covering Africa, West-Asia and North-East Brazil), completed in the year 2003. Three years (2000, 2001 and 2002) of half-hourly data are now available at the local DLR atmospheric data archive. Using the archive satellite data, the hourly cloud cover data with a resolution of $10 \text{ km} \times 10 \text{ km}$ at the nadir was produced. This cloud cover information was stored in a Cloud-Index data set indicating the fraction of transparent atmosphere. Additional data of aerosol optical thickness (monthly climatological values), water vapour, precipitable water (daily values) and ozone (monthly values) were stored at the local DLR archive and were prepared for use. Meteosat-7 calculated the Global Horizontal Irradiation (GHI) using the clear-sky model developed by the SWERA-partner SUNY (State University of Albany, New York) implemented in the DLR-algorithm. The hourly values of solar radiation were integrated to monthly and annual values of the average daily total sum of solar radiation in $\text{Whm}^{-2}\text{day}^{-1}$. The DLR datasets together with methodologies from SUNY for Global radiation were used to develop high resolution maps. Solar radiation data was also prepared

for specific sites for the SWERA project (Schillings et al., 2004).

3.3 Model Description and Estimation

The modified Angstrom-Prescott sunshine model used in the study, is shown below:

$$H = 0.25 H_o + 0.5 H_o(n/N) \quad (3.1)$$

where H ($\text{MJm}^{-2}\text{day}^{-1}$) and H_o ($\text{MJm}^{-2}\text{day}^{-1}$) are the monthly average daily Global solar radiation and extraterrestrial radiation respectively, n is the monthly average daily bright sunshine hours obtained from the Ghana Meteorological Organisation, N is the maximum possible monthly average daily sunshine hours or the day length in hours. The model is based on the assumption that, there exists a linear relationship between: (i) a ratio of bright sunshine hours to astronomical day length and (ii) ratio of incoming daily global solar radiation to the daily extra-terrestrial radiation. This linear relationship is described by empirical model coefficients: a as intercept and b as slope. Both astronomical day length and daily extra-terrestrial radiation are calculated based on location and time (Bojanowski et al., 2013) .

The ratio H/H_o is called the clearness index. It is a dimensionless quantity, and brings out greater clarity for global radiation variations due to climate impacts, i.e. site altitude, site cloudiness and atmospheric turbidity (Diabate et al., 2004). A typical value of this ratio for Wa in the savanna zone of the study area is 0.55 . That means that 55% of the extraterrestrial irradiation reaches the ground.

The ratio n/N is referred to as cloudless index. It gives information about atmospheric characteristics and conditions of the study area (Srivastava and Pandey, 2013).

The constants 'a' and 'b' are the site-specific model parameters. Unfortunately, no

physically based approach has been proposed to determine the parameters. The most common way is to directly calibrate the parameters using observed data. However, the calibration cannot be carried out in many cases because of lack of observed radiation data (Yang and Koike, 2005). In this study the values of $a = 0.25$ and $b = 0.5$ were used as recommended by Allen et al. (1998) based on experimental data collected around the world.

3.3.1 Angle of Declination

The plane of the earth's revolution is referred to as the ecliptic. The earth's axis of rotation is tilted 23.45° from the normal to the plane of the ecliptic (Fig.3). The angle between the plane of the earth's equator and the ecliptic (or the earth - sun line) is the angle of declination δ and it varies between $+23.45^{\circ}$ on June 22 (northern solstice) and -23.45° on December 22 (southern solstice) (Szokolay, 1996) . The angle of declination δ , on a particular Julian day of the year, is computed by:

$$\delta = 23.45 \sin \left(360^{\circ} \times \frac{284 + J}{365} \right) \quad (3.2)$$

where J is the Julian day of the year with January 1st = 1. On equinox days (approximately March 22 and September 21) the earth-sun line is within the plane of the equator, thus $\delta = 0^{\circ}$.

3.3.2 Sunset hour Angle

The hour angle, ω , is the angular distance between the meridian of the observer and the meridian whose plane contains the sun. Thus, the hour angle is zero at local noon (when the sun reaches its highest point in the sky), and increases by 15 degrees. The

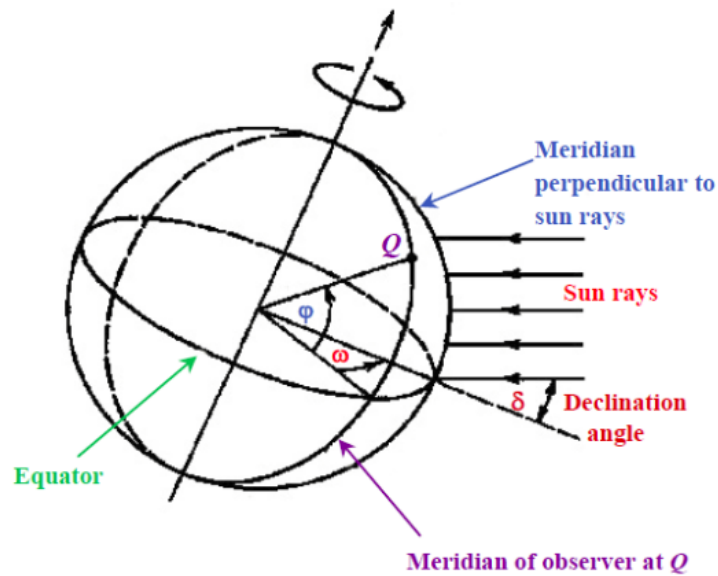


Figure 3.3: The rotation of Earth about its axis, showing the angle of declination (δ), and the sunset hour angle (ω).

sunset hour angle is given by the equation:

$$\omega = \cos^{-1}(-\tan \phi \tan \delta) \quad (3.3)$$

where ϕ is the latitude of the point location on the earth surface in degrees ($^{\circ}$), and δ is the angle of declination in degrees ($^{\circ}$). Additional angles that describe the position of the sun in the sky, as described by Duffie and Beckman (1980) are as follows:

- (i) **Zenith angle** θ_z , the angle between the vertical and the line to the sun, that is, the angle of incidence of beam radiation on a horizontal surface.
- (ii) **Solar altitude angle** α_s , the angle between the horizontal and the line to the sun, that is, the complement of the zenith angle.

3.3.3 Extraterrestrial Solar Flux

This is the amount of solar irradiance at the outer “edge” of the Earth’s atmosphere (Whiteman and Allwine, 1986). Part of this solar radiation penetrates through the

atmosphere to the Earth's surface, while part of it is scattered and/or absorbed by the gas molecules, aerosol particles, cloud droplets and cloud crystals in the atmosphere (Jarraud, 2008). The monthly mean daily extraterrestrial radiation R_o ($\text{MJm}^{-2}\text{day}^{-1}$) is estimated based on Duffie and Beckman (1980) as:

$$R_o = \frac{24 \times 60}{\pi} G_{sc} d_r \left(\omega_s \sin \varphi \sin \delta + \cos \varphi \cos \delta \sin \omega_s \right) \quad (3.4)$$

where G_{sc} is the Solar constant in $\text{MJm}^{-2}\text{min}^{-1}$ and d_r is the relative Earth–Sun distance in metres (m).

3.3.4 Clearness Index

The clearness index (\bar{K}_T) is defined as the ratio of measured global solar radiation (R_g) at ground to the extraterrestrial global solar radiation (R_o) (Poudyal et al., 2012).

$$\bar{K}_T = \frac{R_g}{R_o} \quad (3.5)$$

The \bar{K}_T is an indicator of the relative clearness of the atmosphere, hence the transmittance of the atmosphere and a measure of the amount of solar radiation reaching the study area. According to de Carvalho Alves et al. (2013), a cloudy sky is defined for a range $0 < \bar{K}_T < 0.3$, and a clear sky between $0.65 < \bar{K}_T < 1.0$.

3.3.5 Length of Day

Day length is the time interval in hours between the rising of the sun at the eastern horizon, and the setting of the sun at the western horizon (Forsythe et al., 1995).

Various models have been proposed to estimate the length of each day within the year,

but a more robust and widely used model is presented in equation 3.6 by Forsythe et al. (1995).

$$N = \frac{2}{15} \cos^{-1}(-\tan \phi \tan \delta) \quad (3.6)$$

3.3.6 Performance test for Proposed Model Constants

Based on measurements made at various locations on the Earth, Allen et al. (1998) recommended the values of $a = 0.25$ and $b = 0.50$ in estimating H , when there is available data on sunshine duration but no direct measurements of H .

Anane-Fenin (1986) also proposed three sets of a and b for three regional divisions for the study area, namely Coastal south ($a = 0.267$ and $b = 0.463$), Central region ($a = 0.247$ and $b = 0.420$) and Northern region ($a = 0.290$ and $b = 0.730$).

The performance of Allen's proposed constants and Anane's constants were tested using statistical methods, for some selected sites with measure data from the literature. The statistical tests showed relatively lower RMSE (1.37–2.32) and MPE (2.84–13.24) for the constants from Allen et al. (1998).

Estimation of Solar Radiation

The best proposed constants based on the results of the statistical test, were employed in the model estimation. The final model for the estimation becomes:

$$H = \left(0.25 + 0.5 \frac{n}{N} \right) \left[\frac{24 \times 60}{\pi} G_{sc} d_r \left(\omega_s \sin \varphi \sin \delta + \cos \varphi \cos \delta \sin \omega_s \right) \right] \quad (3.7)$$

where the box bracket is the extraterrestrial solar radiation described in equation 3.4.

3.4 Validation

Six statistical methods were used to test for agreement between the estimated dataset and the DLR satellite data. According to Quansah et al. (2014), Khalil and Shaffie (2013), the Root Mean square Error (RMSE), Mean Bias Error (MBE), Relative Mean Difference (RMD), Mean Percentage Error (MPE), Pearson's Correlation Coefficient (r), t-Test statistic (t) are given in order of Equations 3.3 to 3.8.:

$$\text{RMSE} = \sqrt{\frac{1}{n} \sum_{i=1}^n (G_{\text{cal}} - G_{\text{sat}})^2} \quad (3.8)$$

$$\text{MBE} = \frac{1}{n} \sum_{i=1}^n (G_{\text{cal}} - G_{\text{sat}}) \quad (3.9)$$

$$\text{RMD} = \frac{\frac{1}{n^2} \sum_{i=1}^n |G_{\text{cal}} - G_{\text{sat}}|}{\mu_{\text{cal}}} \quad (3.10)$$

$$\text{MPE} = \frac{1}{n} \sum_{i=1}^n \left(\frac{G_{\text{sat}} - G_{\text{cal}}}{G_{\text{sat}}} \times 100\% \right) \quad (3.11)$$

$$r = \frac{\sum_{i=1}^n (G_{\text{cal}} - \mu_{\text{cal}})(G_{\text{sat}} - \mu_{\text{sat}})}{(n-1)S_{\text{cal}}S_{\text{sat}}} \quad (3.12)$$

$$t = \sqrt{\frac{(n-1)\text{MBE}^2}{\text{RMSE}^2 - \text{MBE}^2}} \quad (3.13)$$

where G_{cal} and G_{sat} are the estimated and satellite values respectively ($\text{MJm}^{-2}\text{day}^{-1}$), for n number of observations. μ is the arithmetic mean and S is the standard deviation.

The value of RMSE is always positive, representing zero in the ideal case. The

smaller the value is, the better the model's performance is (Khalil and Shaffie, 2013).

The MBE provides a clue to whether a given model has a tendency to under-or over-predict, with MBE values closest to zero being desirable. The MPE indicates the percentage deviation of the predicted and measured monthly average daily global solar radiation data (Quansah et al., 2014).

The smaller values of t-statistic are, the better the performance of model. The values of the t-statistic test can be obtained as described in Khalil and Shaffie (2013).

Chapter 4

RESULTS AND DISCUSSIONS

4.1 Clearness Index over Ghana

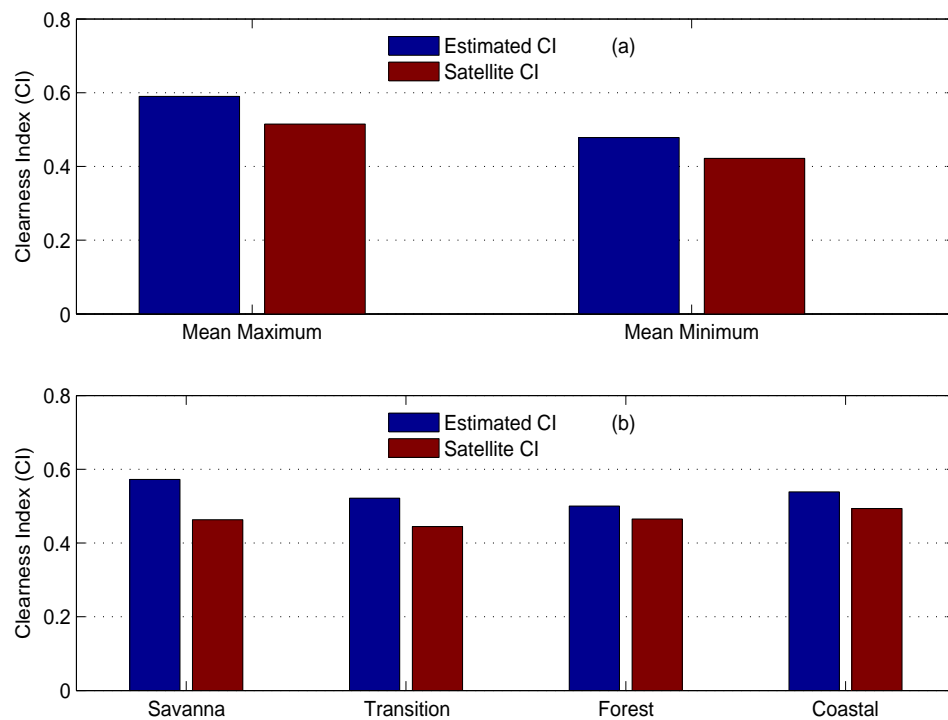


Figure 4.1: Clearness Index (CI) over Ghana: (a) represents the monthly mean maximum and minimum CI over the country and (b) represents Clearness Index (CI) for all the four agro-ecological zones.

The transparency of the atmosphere over Ghana is an all important parameter, for the solar radiation potential of the country. It is indicated by the fraction of extraterrestrial solar radiation which reaches the earth surface as global radiation, and thus is a measure of the degree of the clearness of the sky, or the Clearness Index (Ahmed and

Shaikh, 2013). Figure 4.1 shows the clearness index over Ghana for both estimated and satellite datasets.

It is shown in Figure 4.1(b) that clearness index has an estimated value greater than 50% for all the four agro-Meteorological zones. The monthly average maximum and minimum estimated clearness index for the study area is 59% and 47.8%. This indicates a moderately transparent sky across the country. The Forest zone however, shows the lowest clearness index value of 54%. This is not unexpected as it can be attributed to a bi-modal heavy rainfall and very low temperature regimes over the region (Nkrumah et al., 2014; Owusu and Waylen, 2009). The atmosphere here is thus characteristically moisture laden, with relatively high convective atmosphere. This affords the zone a greater effect of atmospheric attenuation hence low atmospheric transparency.

The low rainfall regime over the Savanna ecological zone, coupled with very low relative humidity and high temperatures, reflect the high levels of Global horizontal insolation over the zone (see Figure 4.1).

The implication of having mean clearness index greater than fifty percent is that the sky is moderately transparent throughout the study area, confirming clear sky conditions and show that the amount of solar radiation on a horizontal surface is sufficient for solar energy utilization in Ghana.

The satellite clearness index is relatively low compared with the estimated clearness index. This is expected since the Meteosat-7 satellite observed Global Horizontal Irradiation, (GHI) by the clear-sky model developed by the SWERA-partner SUNY (State University of Albany, New York), which was implemented in the DLR-

algorithm (Schillings et al., 2004). This model parameterises cloud index, aerosol optical thickness and precipitable water.

The Ångström–Prescott sunshine based model employed in this study however, is primarily a representation of the linear correlation between the ratio of bright sunshine hours to astronomical day length, and ratio of incoming daily global solar radiation to the daily extra-terrestrial radiation. Atmospheric conditions such as aerosol optical thickness and relative humidity are not parameterised in the Ångström–Prescott (A–P) model. This may have accounted for the slight percentage difference observed between the satellite and the estimated data.

Poudyal et al. (2012) reported this observation with the DLR satellite dataset, when compared with estimated and ground measured solar radiation data for the Trans-Himalayan region in Nepal, a member country with the SWERA project.

In addition, studies by Reid (1986) and Tahâş et al. (2011) has proven, that the A-P model coefficients a and b , are not constant values. They are site specific and change considerably with space and time. The more specific the coefficients for a particular geographical site, the better the model estimation. It is therefore expected that a generalisation of a pair of model coefficients over a large area may estimate Global solar radiation with some variation from a site specific estimation.

4.2 Estimated Monthly Trend of Global Solar Radiation over the Agro–Ecological Zones

4.2.1 The Savanna Zone

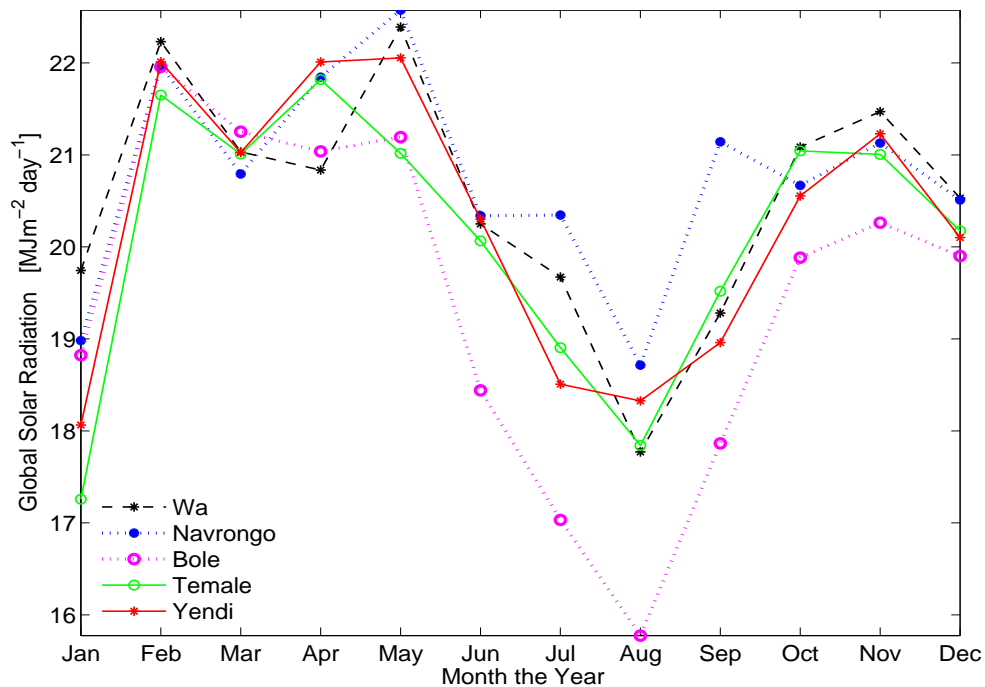


Figure 4.2: Estimated Annual Global Solar Radiation Trend for the five sites in the savanna zone of the study area (Wa, Navrongo, Bole, Temale, and Yendi).

A mean daily Global solar radiation of $20.22 \text{ MJm}^{-2}\text{day}^{-1}$ equivalent to 234 Wm^{-2} is estimated for the savanna zone, with Navrongo having the highest insolation ($22.57 \text{ MJm}^{-2}\text{day}^{-1}$) equivalent to 261.278 Wm^{-2} . The zone experiences the highest insolation during the dry periods of the year for a sustained four month period (February to May), and then suffers a decline. Apparently the lowest insolation levels were estimated for the wet period of the zone from June to September. August is exclusively the month with the lowest estimated insolation. The significantly reduced insolation levels at this time of the annual period, coincides with the period of heavy rainfall

season for the zone. The atmosphere at this time of the year is largely moisture laden, with an abundance of precipitation clouds and an overall increase in convective turbulence. This state of the atmosphere increases attenuation of solar radiation by absorption.

4.2.2 The Transition Zone

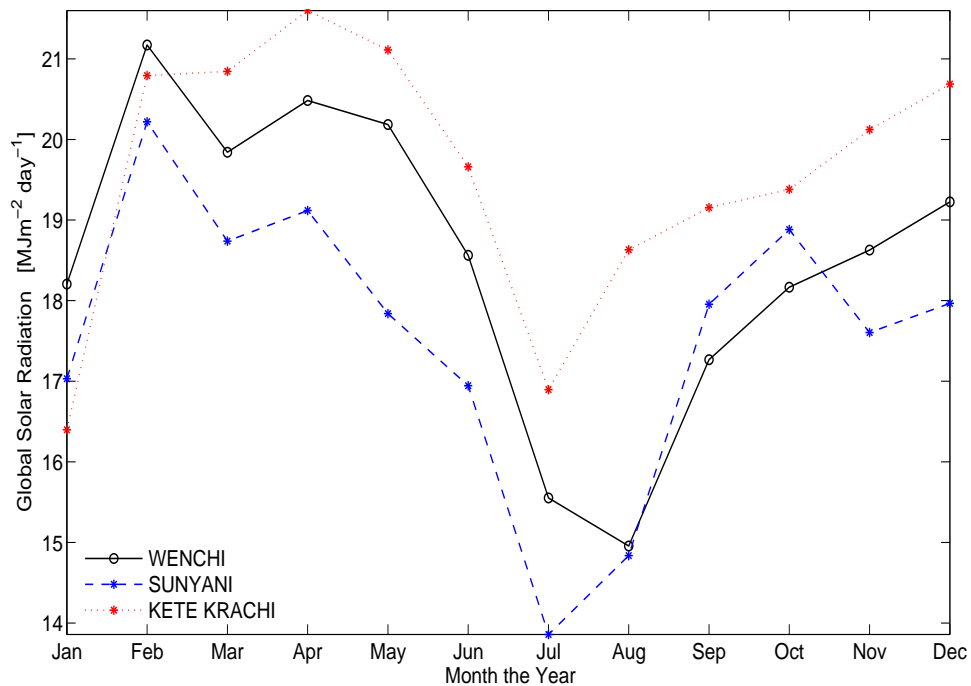


Figure 4.3: Estimated Annual Global Solar Radiation Trends for the three sites in the Transition zone of the study area (Wench, Sunyani, and Kete Krachie).

In the transition zone, Global solar Irradiance increases at the commencement of the annual period from January to a maximum in February. This maximum insolation is shortly sustained for a three month period (February to April) and then suffers a sharp decline in May.

The model estimated a relatively lower daily mean Global solar irradiance of $18.57 \text{ MJm}^{-2}\text{day}^{-1}$ equivalent to 215 Wm^{-2} , compared with the savanna zone. In this zone as with the savanna, the lowest insulations were estimated for the wet periods of the year, between July and August. With a monthly mean clearness index of 57% and an annual mean GSR range between $21.6 \text{ MJm}^{-2}\text{day}^{-1}$ and $15.8 \text{ MJm}^{-2}\text{day}^{-1}$, the zone receives good amounts of solar radiation within an annual period.

4.2.3 The Forest Zone

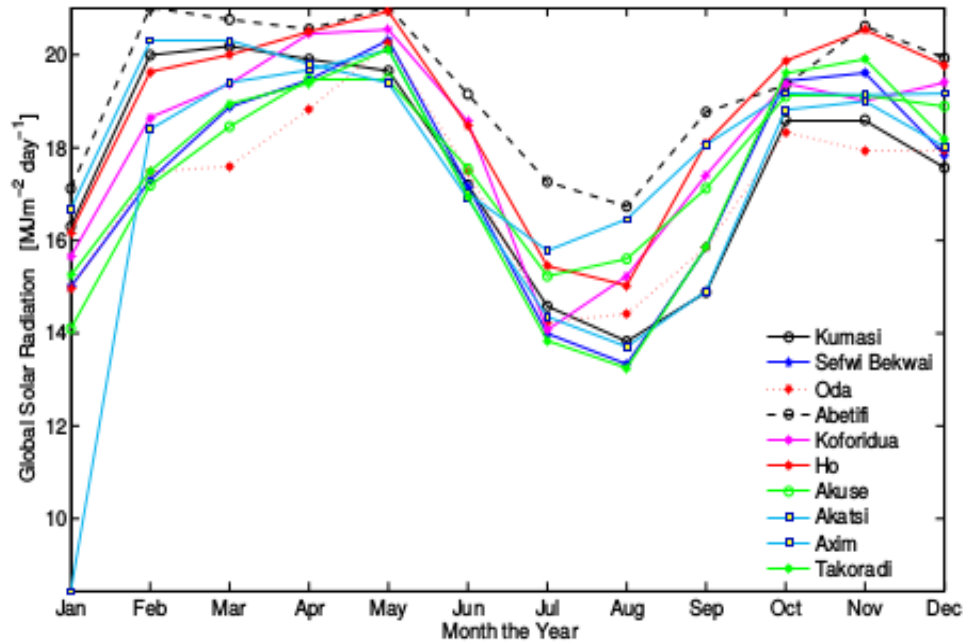


Figure 4.4: Estimated Annual Global Solar Radiation Trends for the eighth sites in the Forest zone of the study area (Kumasi, Sefwi Bekwai, Oda, Abetifi, Koforidua, Ho, Akuse, Akatsi, Axim, and Takoradi).

The Forest zone displays for its annual pattern two distinct periods of maximum Global solar insolation: A longer period of maximum solar insolation (between $19.5 \text{ MJm}^{-2}\text{day}^{-1}$ and $21.0 \text{ MJm}^{-2}\text{day}^{-1}$) dominates the zone in the first half of the year (February - May) and a very shot period of relatively lesser insolation (between $17.9 \text{ MJm}^{-2}\text{day}^{-1}$ and $20.5 \text{ MJm}^{-2}\text{day}^{-1}$) within the last half of the year (October/November). The two periods of maximum insolation are separated distinctly by a depression of minimum insolation ($8.44 \text{ MJm}^{-2}\text{day}^{-1}$). This minimum insolation period perfectly coincides with the regime of maximum precipitation for the zone (June - August). The lowest monthly mean Global solar radiation ($8.44 \text{ MJm}^{-2}\text{day}^{-1}$) was estimated for Akatsi in the south east of the zone. The model estimated the lowest insolation range (between $21 \text{ MJm}^{-2}\text{day}^{-1}$ and 8.4

MJm⁻²day⁻¹) for this zone. Even with so much precipitation clouds, a maximum and minimum clearness index of 54% and 47.8% respectively was estimated for the region (see Figure 2.2(b)) . This means an average of slightly greater than 50% of incoming extraterrestrial Global solar irradiance still reaches the ground.

4.2.4 The Coastal Zone

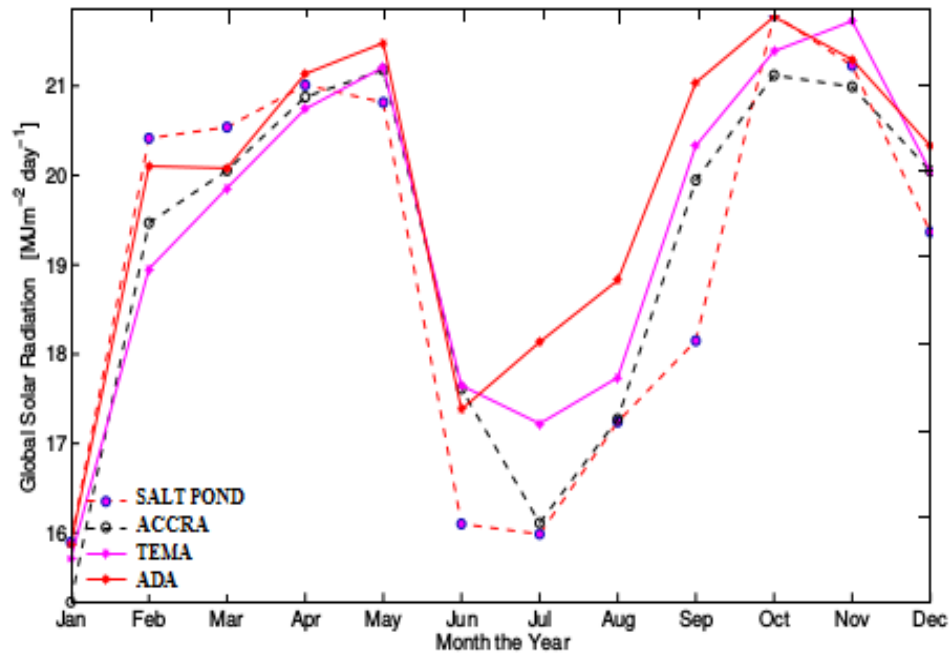


Figure 4.5: Annual Global Solar Radiation Trends for the five sites in the Coastal belt of the study area (Salt Pond, Accra, Tema, and Ada).

In the Coastal zone, the model estimated a relatively higher insolation range (between $21.8 \text{ MJm}^{-2}\text{day}^{-1}$ and $12.4 \text{ MJm}^{-2}\text{day}^{-1}$) compared with the Forest zone. A maximum longer period of solar insolation (between $20.3 \text{ MJm}^{-2}\text{day}^{-1}$ and $21.79 \text{ MJm}^{-2}\text{day}^{-1}$) dominates the zone in the first half of the year (February - May), and a shorter period of relatively maximum insolation (between $18.5 \text{ MJm}^{-2}\text{day}^{-1}$ and $21.3 \text{ MJm}^{-2}\text{day}^{-1}$) within the last half of the year (October/November). The lowest insolation is estimated for the major rainfall period, with estimates between $12.4 \text{ MJm}^{-2}\text{day}^{-1}$ and $15.4 \text{ MJm}^{-2}\text{day}^{-1}$. The estimated Global solar radiation over the Coastal zone is generally higher compared to the Forest zone. Also the Coastal zone has a greater estimated clearness index (0.539) than the Forest zone (0.500). The implication is that Coastal zone has a more transparent sky than that of the Forest

zone. This could be attributed to the relatively observed lower precipitations over the Coastal zone stipulated by Owusu and Waylen (2009).

4.2.5 Estimated and Satellite Annual Global Solar Radiation

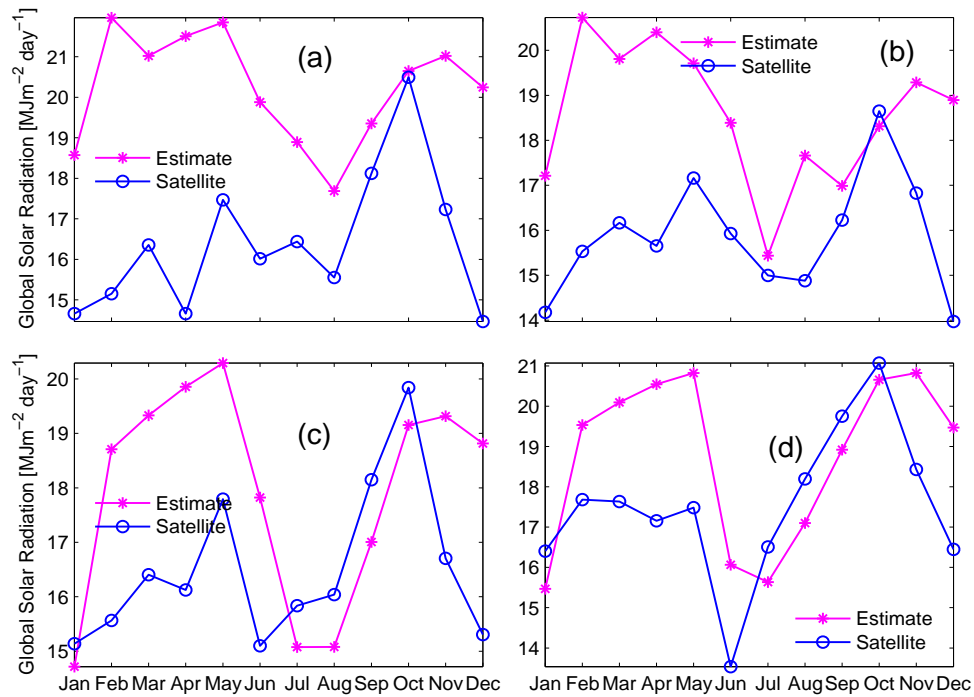


Figure 4.6: Comparing Estimated GSR from the A-P model, and Satellite GSR from the DLR (a) represents the Savana zone, (b) represents the Transition zone, (c) represents the Forest zone, and (d) represents the Coastal zone.

Figure 4.6 compares the estimated results to the Satellite data for an annual period of Global solar radiation distribution over the four agro-ecological zones in the country. The two datasets observe low levels of solar radiation for the peak harmattan (January) and rain seasons (June-August) for each zone, with the highest levels of solar radiation between the two seasons. This observation is attributed to the aerosol (heavy dust) scattering and convective clouds respectively over the country. The model estimated for the harmattan season, insolation levels between $14.7 \text{ MJm}^{-2}\text{day}^{-1}$ and $18.8 \text{ MJm}^{-2}\text{day}^{-1}$ across the nation, with mean satellite observation of $14.18 \text{ MJm}^{-2}\text{day}^{-1}$. The period between June and August, also observed a mean low insolation between $15.1 \text{ MJm}^{-2}\text{day}^{-1}$ and $13.5 \text{ MJm}^{-2}\text{day}^{-1}$ for both

model estimation and satellite data.

Between the two seasons (namely harmattan and rain), high insolation levels ranging from $20.3 \text{ MJm}^{-2}\text{day}^{-1}$ to $21.97 \text{ MJm}^{-2}\text{day}^{-1}$ are estimated by the A-P model, and $18.65 \text{ MJm}^{-2}\text{day}^{-1}$ to $21.1 \text{ MJm}^{-2}\text{day}^{-1}$ for satellite observations. These results are consistent with the clearness index analysis discussed in section 4.1, affirming that the country is abundantly irradiated for the clear sky periods of the year, namely February to May, and also October. The results from the statistical tests (Root Mean Square Error (RMSE)), Mean Bias Error (MBE), Relative Mean Difference (RMD), and Absolute Mean Percentage Error (AMPE)) discussed in the validation section show that a credibly good agreement exists between the two observations.

4.3 Gridded Estimated Global Solar Radiation

4.3.1 Monthly Horizontal Insolation

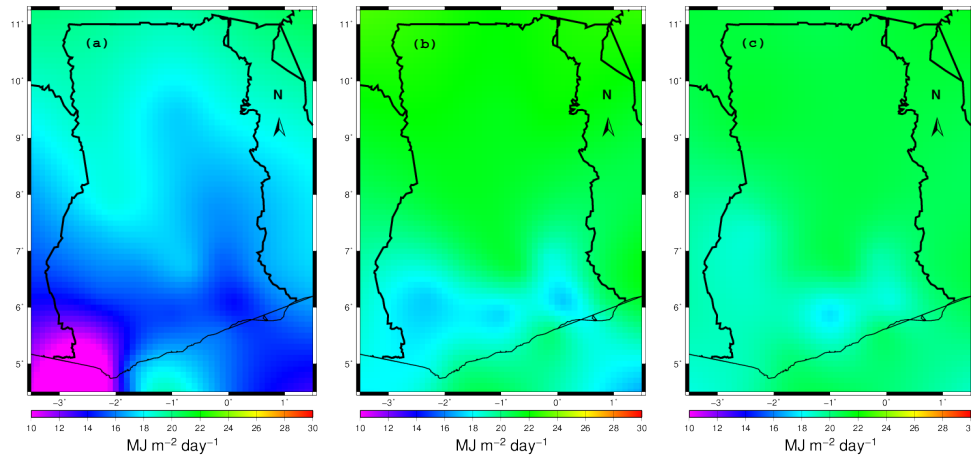


Figure 4.7: Gridded Monthly Mean Global Solar Irradiance: (a) represents January, (b) represents February, and (c) represents March.

January (Figure 4.7a) falls within the peak period of the Harmattan season (Sunnu, 2012). During that period storm activities in the Bilma and Faya Largeau area in the Chad basin raise large amounts of dust into the atmosphere, which is then carried south-west by the predominant winds. As the Intertropical Convergence Zone (ITCZ) in December to February is located in the southern part of Ghana, or in the Atlantic Ocean but close to the coast of the Gulf of Guinea, the Harmattan wind stops there and most of the dust settles over the region (He et al., 2007).

Tserenpurev et al. (2012) and Mikami et al. (2006) have shown that Solar radiation decreases in dust days due to the scattering and absorption by dust aerosols. This is the case for the country in January. A phenomenal increase in aerosol scattering and absorption increases the effect of attenuation, decreasing sunshine intensity and

hence the amount of ground insolation. This is further demonstrated by the fact that, the harmattan season is characterized by a very cold dry (9° C) wind, due to decreased short-wave solar radiation absorption at the ground (Minka and Ayo, 2014) . The model estimated a monthly mean Global solar radiation of $16.14 \text{ MJm}^{-2}\text{day}^{-1}$ in January over the country.

February (Figure 4.7b) is largely the closing period for the harmattan season. During the period, the more denser dust particles have settled to the ground and water bodies, leaving only the finer once mostly over the south. The effect of attenuation has significantly reduced over the country, with the ITCZ still to migrate from the coast. During this period, average solar radiation levels across the country will begin to increase further. This is clearly the case as shown in section 4.2. February commences the period of the year with maximum levels of solar radiation for all four agro–ecological zones across the country. The very fine dust particles still suspended in the atmosphere as intimated by He et al. (2007), may be partly responsible for the relatively lower solar radiation levels shown in some areas of the Forest zone.

In March (Figure 4.7c), the atmosphere is relatively clearer with significantly reduced aerosol concentration. The clearness index over the country reaches 55% for this period. The country receives increasing levels of solar radiation, especially for the savanna zone. At this time the Convergence zone is gradually migrating inland and the atmosphere is becoming clean and moist.

April (Figure 4.8a) is also a month with a cleaner and more transparent atmosphere. There is a nation-wide irradiance with some degree of atmospheric opacity in a few areas of the Forest belt. In general February, March, April and May, are the peak solar radiation periods of across the study area.

May (Figure 4.8b) continues with the longer annual first half maximum irradiance periods (February to May). A monthly mean Clearness index of 56% is estimated for the month. The west coast in the Transition zone still offers some attenuation.

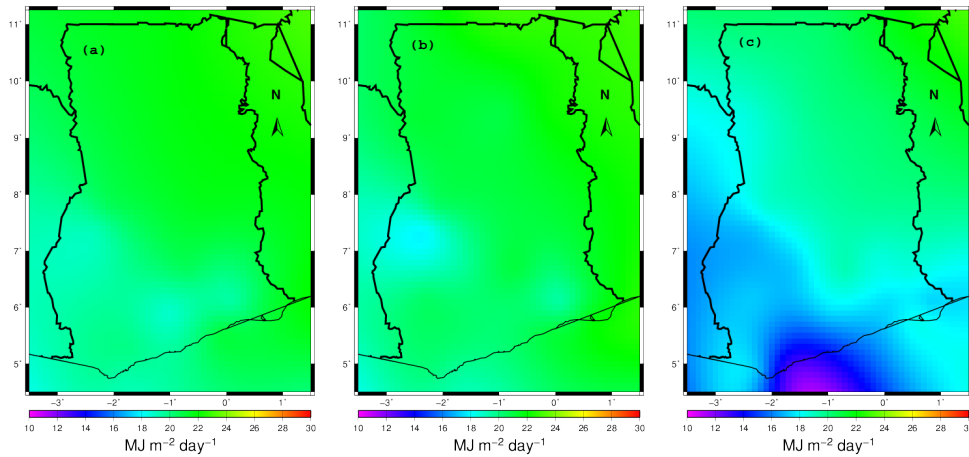


Figure 4.8: Gridded Monthly Mean Global Solar Irradiance: (a) represents April, (b) represents May, and (c) represents June

By June (Figure 4.8c) the ITCZ is well migrated into the country. The southern regions experience much convective activities. The atmosphere over the south is very moist laden, once again increasing attenuation by water vapour.

In July (Figure 4.9a) the lowest mean clearness index of 45% is estimated. These are very heavy rain periods for most parts of the country, and consequentially very cloudy atmospheres over the subregion.

By July (Figure 4.9a) and August (Figure 4.9b) rains have covered the entire nation, rendering the atmosphere wet and moisture laden throughout. There is increased attenuation of solar radiation, due mostly to water vapour.

In September (Figure 4.9c) the ITCZ is receding, leaving the atmosphere relatively clearer from the north than the much moisture laden rainfall regime. The atmosphere is still very moist over the Forest and Coastal zones, with estimated solar radiation of $17 \text{ MJm}^{-2}\text{day}^{-1}$ and $18.9 \text{ MJm}^{-2}\text{day}^{-1}$. In October (Figure 4.10a)

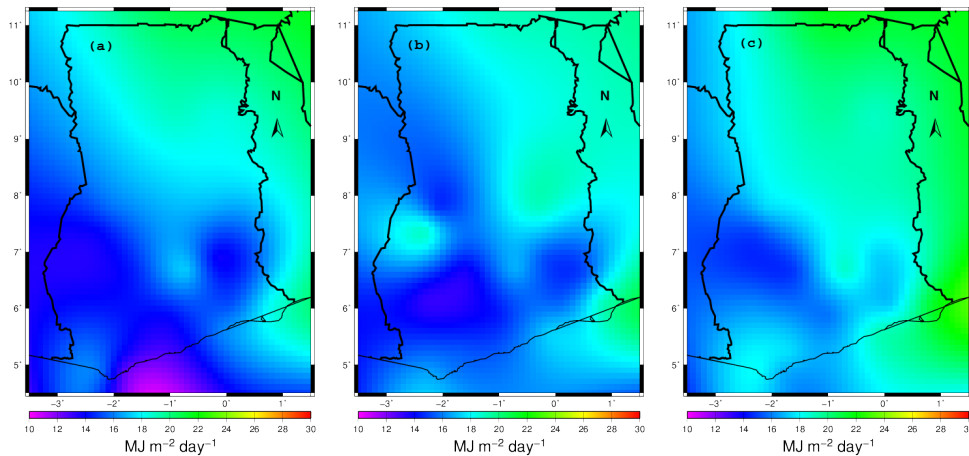


Figure 4.9: Gridded Monthly Mean Global Solar Irradiance: (a) represents July, (b) represents August, and (c) September.

when the rains have almost diminished, a transparent nationwide atmosphere is restored. The lesser rains over the savanna zone make it possible for increasing solar radiation.

Though November (Figure 4.10b) and December (Figure 4.10c) mark the commencement of the harmattan season, the very denser dust particles are yet to take over the entire nation. The phenomena is gradual, and finds its peak in January when the atmosphere of the entire country densely laden with dust, with very pronounced aerosol scattering and absorption.

October and November afford the country with relatively short but highly transparent atmosphere (with clearness index reaching 60% in November). The country receives very well insolation levels though for a short period just prior to the peak harmattan.

The estimated datasets show a downward trend of Global solar radiation from Octo-

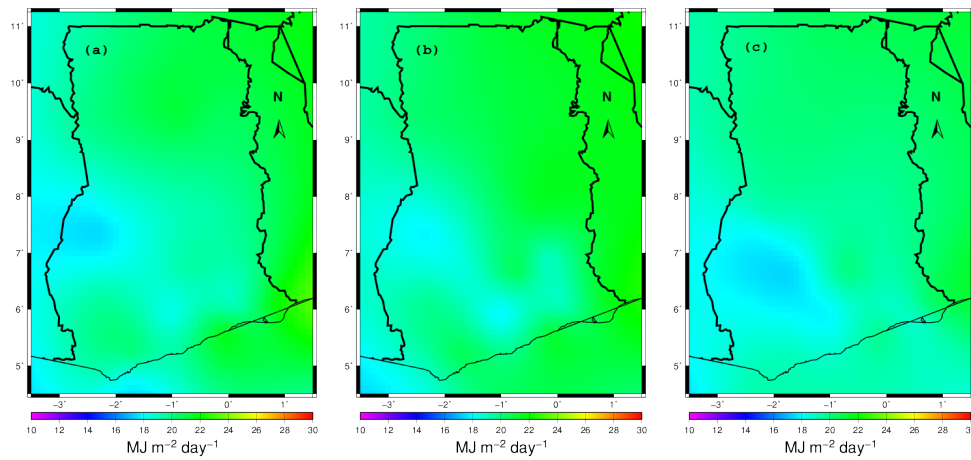


Figure 4.10: Gridded Monthly Mean Global Solar Irradiance: (a) represents October, (b) represents November, and (c) December.

ber to December (October = $21.8 \text{ MJm}^{-2}\text{day}^{-1}$, November = $21.5 \text{ MJm}^{-2}\text{day}^{-1}$, and December = $20.5 \text{ MJm}^{-2}\text{day}^{-1}$)

4.3.2 Annual Horizontal Insolation

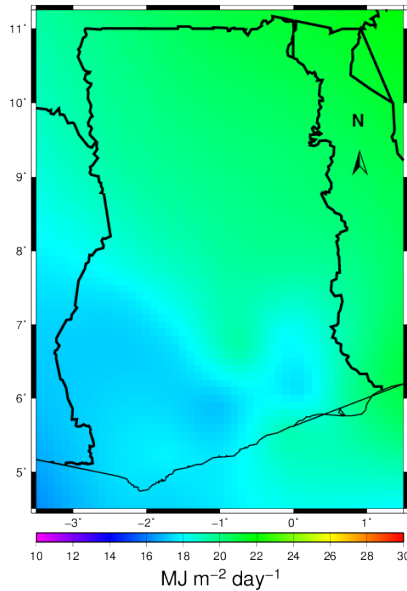


Figure 4.11: Gridded Annual mean Global Solar Irradiance.

Figure 4.11 illustrates the estimated annual mean Global Solar irradiance over the four agro-ecological zones of Ghana. It is observed that the country is very well irradiated with the northern half (Savanna and Transition zones) receiving the highest amount of Global solar radiation ($22.57 \text{ MJm}^{-2}\text{day}^{-1}$) equivalent to (261.278 Wm^{-2}), and the southern half, typically the forest zone, receiving the lowest levels of insolation ($8.44 \text{ MJm}^{-2}\text{day}^{-1}$) equivalent to (97.69 Wm^{-2}). This is attributed to low clearness indices. The atmosphere over the zone is highly moisture laden and cloudy, with much convective turbulence. This is further supported by the fact that the Forest zone records the highest amount of annual mean rainfall.

4.3.3 Validation of Estimated Global Solar Radiation

The Satellite Global solar radiation datasets were obtained at a $10 \text{ km} \times 10 \text{ km}$ spatial resolution. The model estimated datasets have thus been gridded for a $10 \text{ km} \times 10 \text{ km}$ spatial resolution to enable a statistical performance assessment of the model.

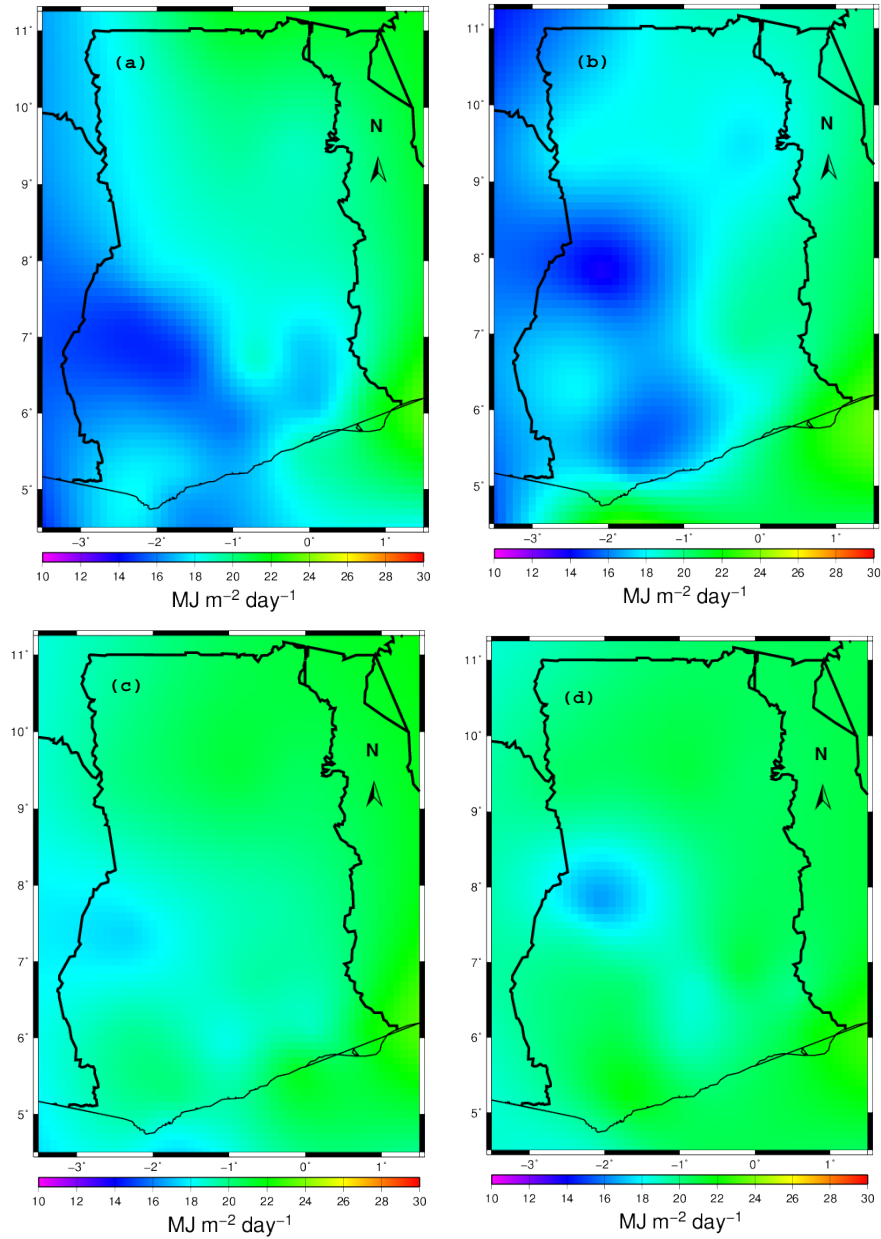


Figure 4.12: Gridded Monthly Mean Global Solar Irradiance: (a) represents Estimated GSR for September, (b) represents Satellite GSR for September (c) represents Estimated GSR for October and (d) represents Satellite GSR for October.

From the various statistical tests conducted, good agreement was observed between

the estimated grids and satellite grid. Very few deviations were shown between the grids of the two datasets. The model often had slightly greater estimated solar radiation. This is attributed to the fact that, the Meteosat-7 satellite observed solar radiation as function of aerosol opacity and cloud cover, quantities not very well captured in the A-P model.

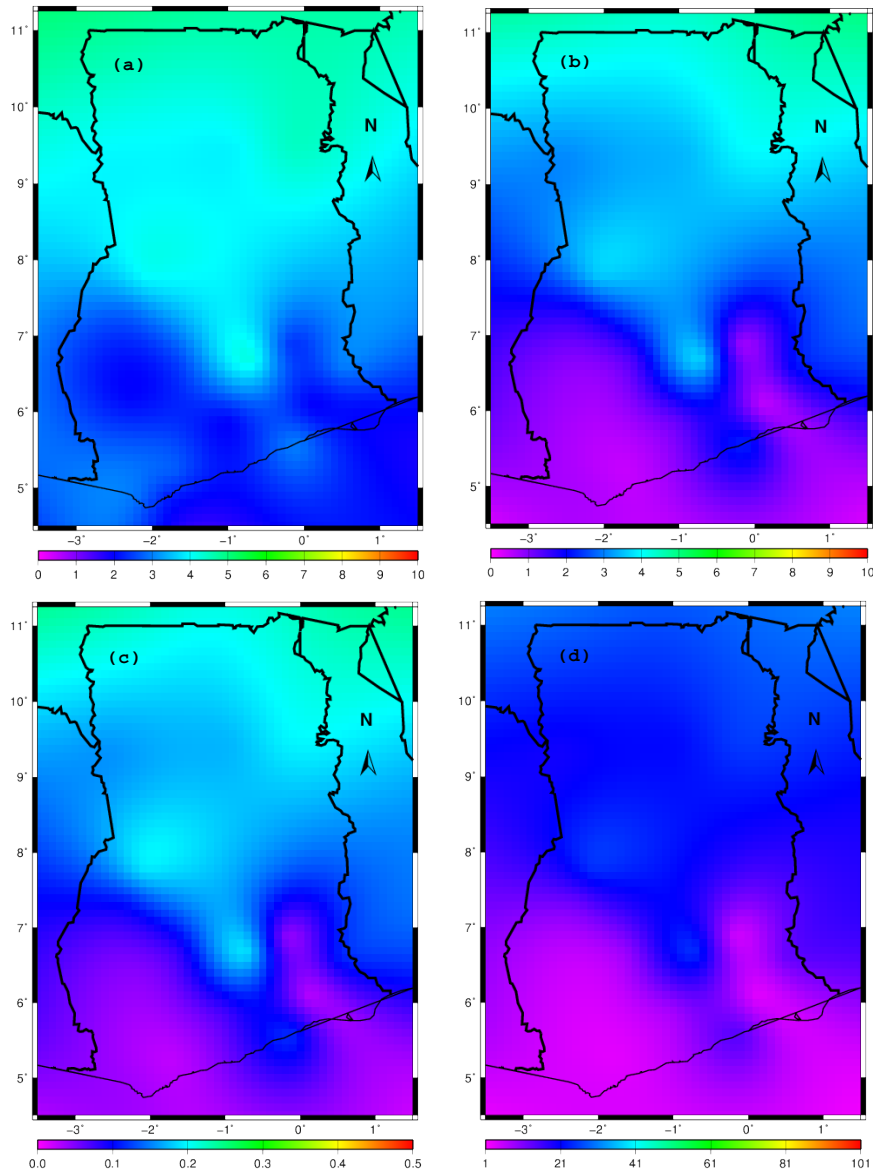


Figure 4.13: Gridded Statistical Tests: (a) represents Root Mean Square Error (RMSE), (b) represents Mean Bias Error (MBE) (c) represents Relative Mean Difference (RMD) and (d) represents Absolute Mean Percentage Error (AMPE).

The root mean square error test (RMSE) was carried out to investigate the statistical difference between the estimated dataset and the satellite dataset. The smaller the

value is, the better the model performance is. Appreciable RMSE values between 1–5 were obtained. This coincides with the RMSE range of most empirical models for estimating Global solar radiation. This strong statistical correlation is further confirmed by low relative mean difference (RMD) (0.03–0.22), and low absolute mean percent error (3–29).

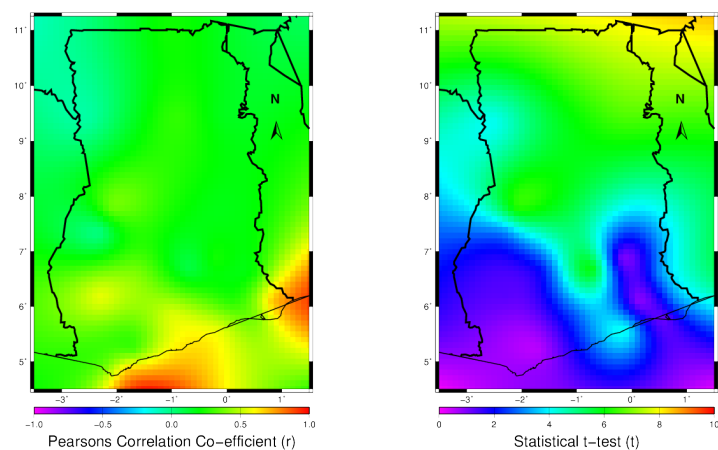


Figure 4.14: Gridded Statistical Tests: Left grid represents the Person’s Correlation Co-efficient; Right grid represents t-statistic test.

The Pearson’s correlation co-efficient test also yielded very good positive results (0.1–0.7). Also the t–statistical test showed the standard low results (0.6–7.5). The agreement between the model and the satellite data is generally strongest in the south. This may be attributed to the greater station density at the south of the country.

4.3.4 Summary of Seasonal and Annual GSR

Table 4.1: Estimated seasonal and annual monthly mean Global Solar radiation for the four agro-ecological zones.

Months	GSR [M J m⁻² day⁻¹]			
	Savana	Transition	Forest	Coastal
Dec-Jan-Feb (DJF)	20.26	18.95	17.41	18.16
Mar-Apr-May (MAY)	21.46	19.97	19.23	20.49
Jun-Jul-Aug (JJA)	18.82	17.16	15.99	16.27
Sep-Oct-Nov (SON)	20.34	18.2	18.49	20.13
Annual	20.22	18.57	17.93	18.76

Table 4.1 summarises the estimated seasonal and annual mean Global Solar radiation for the four agro-ecological zones. Each column represents a monthly mean GSR for the particular zone. The savanna zone and the Forest zone are exclusively the regions with the highest and lowest solar radiation levels respectively. For all the zones, the highest solar radiation levels occur in the second trimester (MAM). The third trimester (JJA) is the period with the lowest solar radiation estimates all over the country. This is attributed to the fact that this particular trimester (JJA) is the main rain season for the country, making the atmosphere heavily laden with clouds and water vapor, hence increased absorption of solar radiation.

Annually, the savanna and the transition zones experience the highest irradiation levels, with the southern belt, chiefly the forest zone experiencing the lowest irradiation levels.

Chapter 5

CONCLUSIONS AND RECOMMENDATIONS

5.1 Conclusions

In this study, the monthly mean Global Solar Radiation (GSR) over Ghana has been estimated from sunshine duration data measured at twenty synoptic stations distributed across the country, using the Ångström–Prescott sunshine duration model. The estimated monthly mean GSR datasets were then gridded at a spatial resolution of $10 \text{ km} \times 10 \text{ km}$, establishing the trend and distribution across the country. In addition, the estimated dataset was compared with available satellite data from the German Aerospace Centre (DLR). The statistical tests show good agreement, with appreciable RMSE values between 1-5, low relative mean difference (RMD) (0.03-0.22), low absolute mean percent error (3-29%), and appreciable Pearson's correlation (0.1-0.7). The results showed that, the estimated total monthly mean Global Solar irradiation over the country is $412.82 \text{ MJm}^{-2}\text{day}^{-1}$ equivalent to 4778.02 Wm^{-2} , with the highest solar radiation estimated for the savanna zone at Navrongo ($20.76 \text{ MJm}^{-2}\text{day}^{-1}$) equivalent to 240.28 Wm^{-2} , and the lowest for the forest zone at Oda ($17.11 \text{ MJm}^{-2}\text{day}^{-1}$) equivalent to 198.03 Wm^{-2} . A maximum and minimum monthly mean clearness index of 0.59 and 0.48 respectively is estimated. This means an estimated 53 % of Solar radiation at the top of the atmosphere reaches the surface of the study area after attenuation. These results agree favorably with

the Global energy budget presented by Wild et al. (2013). Meanwhile, the maximum annual time series GSR over the country are within the dry seasons of the year when the atmosphere is mostly clean from dust, and the minimum annual time series GSR are within the wet and harmattan periods of the year. The satellite data has a total monthly mean Global Solar irradiation of $366.62 \text{ MJm}^{-2}\text{day}^{-1}$ equivalent to 4243.30 Wm^{-2} . The small station number density and poor ability to conserve extrapolation trends by the Minimum Surface Curvature method is apparently an unavoidable limitation to the study.

Notwithstanding, the study shows that solar radiation levels over the country ($17.11 \text{ MJm}^{-2}\text{day}^{-1}$ to $20.76 \text{ MJm}^{-2}\text{day}^{-1}$), meet the international solar technology market standards of $18.7 \text{ MJm}^{-2}\text{day}^{-1}$ to $20.7 \text{ MJm}^{-2}\text{day}^{-1}$ for the operation of photovoltaic systems and solar collectors for industrial and domestic applications

These results may have useful applications in the field of Solar energy technology, with regards to the growing demand for energy in the country, and also to better understand the climate system over Ghana.

5.2 Recommendations

5.2.1 Recommendations for Policy

- The high Global solar radiation levels affirm that Ghana is undoubtedly a potential country for harnessing and promoting solar energy technology. This could resolve the growing demand for energy, thus curtailing the phenomenal power crisis within the country. It is therefore recommended that solar farms should be built across the country especially in the Savanna and Transition zones where radiation levels are highest.
- The lowest levels of Global solar Radiation was estimated for the mid-section period of the year (June - September), when there are heavy rains nationwide, and consequential clouds significantly reducing the clearness index. Solar energy technology investors can harness maximum solar energy countrywide over a longer period of time (February to May) within the first half of the annual period. This energy can be saved for consumption.

5.2.2 Recommendation for Future Research

- Pyranometers should be mounted across the country to collect real-time ground based measurement for Global solar radiation.
- The work was carried out for twenty-two synoptic stations, as the model required sunshine duration which were readily available at the synoptic stations. Further work should be carried out using temperature based models such as the Bristow-Campbell model, with temperature data from both the synoptic and

climatological stations within the country. This will afford a relatively larger station density for estimating and gridding the spatial distribution of Global solar radiation across the country, and also to investigate the Global temperature fluctuation across the country.

Bibliography

- Ahmed, M. A. and Shaikh, S. A. (2013). Solar radiation studies for Dubai and Sharjah, UAE. *World Academy of Science, Engineering and Technology*, 73:1007–1014.
- Allen, R. G., Pereira, L. S., Raes, D., Smith, M., et al. (1998). Crop evapotranspiration-guidelines for computing crop water requirements-fao irrigation and drainage paper 56. *FAO, Rome*, 300(9):D05109.
- Amekudzi, L. K., Yamba, E. I., Preko, K., Asare, E. O., Aryee, J., Baidu, M., and Codjoe, S. N. (2015). Variabilities in rainfall onset, cessation and length of rainy season for the various agro-ecological zones of Ghana. *Climate*, 3(2):416–434.
- Anane-Fenin, K. (1986). Estimating solar radiation in Ghana. Technical report, International Centre for Theoretical Physics, Trieste (Italy).
- Ångström, A. (1924). Solar and terrestrial radiation. report to the international commission for solar research on actinometric investigations of solar and atmospheric radiation. *Quarterly Journal of the Royal Meteorological Society*, 50(210):121–126.
- Arku, F. S. (2011). The modelled solar radiation pattern of Ghana: Its prospects for alternative energy source. *Journal of African Studies and Development*, 3(3):45–64.
- Bojanowski, J. S., Vrieling, A., and Skidmore, A. K. (2013). Calibration of solar

- radiation models for Europe using Meteosat second generation and weather station data. *Agricultural and forest meteorology*, 176:1–9.
- Boyle, G. (1996). *Renewable energy: power for a sustainable future*.
- Chang, J. H. (1974). *Climate and agriculture: an ecological survey*. Transaction Publishers.
- Chen, C. J. (2011). *Physics of solar energy*. John Wiley & Sons.
- Christopherson, R. W. (2014). *Geosystems: an introduction to physical geography*. Pearson Higher Ed.
- Cunningham, W. P., Saigo, B. W., and Cunningham, M. A. (2001). *Environmental science: A global concern*, volume 412. McGraw-Hill Boston, MA.
- de Carvalho Alves, M., Sanches, L., de Souza Nogueira, J., and Silva, V. A. M. (2013). Effects of sky conditions measured by the clearness index on the estimation of solar radiation using a digital elevation model. *Atmospheric and Climate Sciences*, 2013.
- Diabate, L., Blanc, P., and Wald, L. (2004). Solar radiation climate in Africa. *Solar Energy*, 76(6):733–744.
- Disch, D. and Bronckaers, J. (2012). *An analysis of the off-grid lighting market in Rwanda: sales, distribution and marketing*. GVEP International.
- Duffie, J. A. and Beckman, W. A. (1980). *Solar engineering of thermal processes*, volume 3. Wiley New York etc.

- Etier, I., Ababneh, M., and Tarabsheh, A. A. (2011). Simulation of a 10 kw photovoltaic system in areas with high solar irradiation. *American Journal of Applied Sciences*, 8(2):177.
- Fleagle, R. G. and Businger, J. A. (1981). *An introduction to atmospheric physics*, volume 25. Academic Press.
- Forson, F., Agbeko, K., Edwin, I., Sunnu, A., Brew-Hammond, A., and Akuffo, F. (2004). Solar energy resource assessment for Ghana. *Department of Mechanical Engineering, Kwame Nkrumah University of Science and Technology, Kumasi, Ghana*.
- Forsythe, W. C., Rykiel, E. J., Stahl, R. S., Wu, H.-i., and Schoolfield, R. M. (1995). A model comparison for daylength as a function of latitude and day of year. *Ecological Modelling*, 80(1):87–95.
- Gilani, S. I.-u.-H., Dimas, F. A. R., Shiraz, M., et al. (2011). Hourly solar radiation estimation using ambient temperature and relative humidity data. *International Journal of Environmental Science and Development*, 2(3):188–193.
- Gray, L. J., Beer, J., Geller, M., Haigh, J. D., Lockwood, M., Matthes, K., Cubasch, U., Fleitmann, D., Harrison, G., Hood, L., et al. (2010). Solar influences on climate. *Reviews of Geophysics*, 48(4).
- Gültekin, K., Richstone, D. O., Gebhardt, K., Lauer, T. R., Tremaine, S., Aller, M., Bender, R., Dressler, A., Faber, S., Filippenko, A. V., et al. (2009). The m - σ and m l relations in galactic bulges, and determinations of their intrinsic scatter. *The Astrophysical Journal*, 698(1):198.

- Hargreaves, G. H. and Samani, Z. A. (1982). Estimating potential evapotranspiration. *Journal of the Irrigation and Drainage Division*, 108(3):225–230.
- He, C., Breuning-Madsen, H., and Awadzi, T. W. (2007). Mineralogy of dust deposited during the harmattan season in Ghana. *Geografisk Tidsskrift-Danish Journal of Geography*, 107(1):9–15.
- Hejase, H. A. and Assi, A. H. (2011). Time-series regression model for prediction of monthly and daily average global solar radiation in Al Ain city-UAE. In *Global Conference on Global Warming-2011 (GCGW-2011), Lisbon, Portugal, July*, pages 11–14.
- Hewitt, C. N. and Jackson, A. V. (2008). *Handbook of atmospheric science: Principles and applications*. John Wiley & Sons.
- Jarraud, M. (2008). Guide to meteorological instruments and methods of observation (wmo-no. 8). *World Meteorological Organisation: Geneva, Switzerland*.
- Kalogirou, S. A. (2004). Solar thermal collectors and applications. *Progress in energy and combustion science*, 30(3):231–295.
- Kaufman, D. G. and Franz, C. M. (1996). *Biosphere 2000: Protecting our global environment*, Kendall.
- Khalil, S. and Shaffie, A. (2013). Performance of statistical comparison models of solar energy on horizontal and inclined surface. *International Journal of Energy and Power*, 2(1).
- Kwakwa, P. A. (2014). Energy-growth nexus and energy demand in Ghana: A review of empirical studies. *Applied Research Journal*, 1(1).

- Laue, E. (1970). The measurement of solar spectral irradiance at different terrestrial elevations. *Solar Energy*, 13(1):43–57.
- Li, H., Cao, F., Wang, X., and Ma, W. (2014). A temperature-based model for estimating monthly average daily global solar radiation in china. *The Scientific World Journal*, 2014.
- Meinel, A. B. and Meinel, M. P. (1976). Applied solar energy. an introduction.
- Mikami, M., Shi, G., Uno, I., Yabuki, S., Iwasaka, Y., Yasui, M., Aoki, T., Tanaka, T., Kurosaki, Y., Masuda, K., et al. (2006). Aeolian dust experiment on climate impact: An overview of japan–china joint project adec. *Global and Planetary Change*, 52(1):142–172.
- Minka, N. S. and Ayo, J. O. (2014). Influence of cold-dry (harmattan) season on colonic temperature and the development of pulmonary hypertension in broiler chickens, and the modulating effect of ascorbic acid. *Open Access Animal Physiology*, 6.
- Muzathik, A., Nik, W., Ibrahim, M., Samo, K., Sopian, K., and Alghoul, M. (2011). Daily global solar radiation estimate based on sunshine hours. *International Journal of Mechanical and Materials Engineering*, 6(1):75–80.
- Myers, D. R. (2013). *Solar radiation: practical modeling for renewable energy applications*. CRC Press.
- Namrata, K., Sharma, S., and Saksena, S. (2012). Comparison of estimated daily global solar radiation using different empirical models. *International Journal of Science and Advanced Technology*, 2(4).

- Nkrumah, F., Klutse, N. A. B., Adukpo, D. C., Owusu, K., Quagraine, K. A., Owusu, A., Gutowski Jr, W., et al. (2014). Rainfall variability over ghana: Model versus rain gauge observation. *International Journal of Geosciences*, 5(07):673.
- Ogolo, E. (2014). Estimation of global solar radiation in nigeria using a modified angstrom model and trend analysis of the allied meteorological components. *Indian Journal of Radio and Space physics*, 43:213–224.
- Owusu, K. and Waylen, P. (2009). Trends in spatio-temporal variability in annual rainfall in ghana (1951-2000). *Weather*, 64(5):115–120.
- Page, J. (1967). The estimation of monthly mean values of daily total short wave radiation on vertical and inclined surfaces from sunshine records 40s-40n. In *Proc. of UN new sources of energy (Conference paper) Rome*, volume 4, pages 378–90.
- Pandey, C. K. and Katiyar, A. (2013). Solar radiation: Models and measurement techniques. *Journal of Energy*, 2013.
- Paulescu, M., Paulescu, E., Gravila, P., and Badescu, V. (2012). *Weather modeling and forecasting of PV systems operation*. Springer Science & Business Media.
- Peterson, T. C., Easterling, D. R., Karl, T. R., Groisman, P., Nicholls, N., Plummer, N., Torok, S., Auer, I., Boehm, R., Gullett, D., et al. (1998). Homogeneity adjustments of in situ atmospheric climate data: a review. *International Journal of Climatology*, 18(13):1493–1517.
- Poudyal, K., Bhattarai, B. K., Sapkota, B., and Berit, K. (2012). Estimation of global solar radiation using sunshine duration in himalaya region. *Research Journal of Chemical Sciences*, 2(11):20–25.

- Prescott, J. (1940). Evaporation from a water surface in relation to solar radiation. *Transactions of the Royal Society of South Australia*, 64(1940):114–118.
- Quansah, E., Amekudzi, L. K., Preko, K., Aryee, J., Boakye, O. R., Boli, D., and Salifu, M. R. (2014). Empirical models for estimating global solar radiation over the Ashanti region of Ghana. *Journal of Solar Energy*, 2014.
- Quansah, E., Mauder, M., Balogun, A. A., Amekudzi, L. K., Hingerl, L., Bliefernicht, J., and Kunstmann, H. (2015). Carbon dioxide fluxes from contrasting ecosystems in the Sudanian Savanna in West Africa. *Carbon balance and management*, 10(1):1.
- Ramanathan, V. (1987). The role of earth radiation budget studies in climate and general circulation research. *Journal of Geophysical Research: Atmospheres (1984–2012)*, 92(D4):4075–4095.
- Reid, P. (1986). Evaluation of the coefficients of the Ångström formula for the estimation of solar radiation in South Africa. *South African Journal of Plant and Soil*, 3(1):45–48.
- Sarsah, E. A. and Uba, F. A. (2013). Monthly-specific daily global solar radiation estimates based on sunshine hours in Wa, Ghana. *International Journal Of Scientific and Technology Research*, 2:246–254.
- Schillings, C., Meyer, R., and Trieb, F. (2004). Solar and wind energy resource assessment (swera). *High Resolution Solar Radiation Assessment for Kenya. Final country report prepared by DLR–submitted to UNEP/GEF. Nairobi, Kenya.*

- Sivamadhavi, V. and Selvaraj, R. S. (2012). Robust regression technique to estimate the global radiation. *Indian Journal of Radio & Space Physics*, 41(1):17–25.
- Smith, W. and Wessel, P. (1990). Gridding with continuous curvature splines in tension. *Geophysics*, 55(3):293–305.
- Srivastava, R. and Pandey, H. (2013). Estimating angstrom-prescott coefficients for india and developing a correlation between sunshine hours and global solar radiation for india. *ISRN Renewable Energy*, 2013.
- Sunnu, A. K. (2012). Particle size and concentrations of the harmattan dust near the Gulf of Guinea. *Journal of Environmental Science and Engineering. A*, 1(10A):1203.
- Szokolay, S. V. (1996). Solar geometry. PLEA.
- Tahâş, S., Ristoiu, D., and Cosma, C. (2011). Trends of the Global solar radiation and air temperature in Cluj-Napoca, Romania (1984-2008). *Rom J Physiol*, 56(5/6):784–789.
- Tserenpurev, B., Shinoda, M., and Tsubo, M. (2012). Effects of cloud, atmospheric water vapor, and dust on photosynthetically active radiation and total solar radiation in a mongolian grassland. *Journal of Arid Land*, 4(4):349–356.
- Wansah, J., Udounwa, A., Mee, A., and Emah, J. (2014). Comparison of sunshine based models for estimating global solar radiation in uyo, nigeria. *New York Science Journal*, 7(12):60–65.
- Whiteman, C. D. and Allwine, K. J. (1986). Extraterrestrial solar radiation on inclined surfaces. *Environmental Software*, 1(3):164–169.

- Wild, M., Folini, D., Schär, C., Loeb, N., Dutton, E. G., and König-Langlo, G. (2013). The global energy balance from a surface perspective. *Climate dynamics*, 40(11-12):3107–3134.
- Winslow, J. C., Hunt, E. R., and Piper, S. C. (2001). A globally applicable model of daily solar irradiance estimated from air temperature and precipitation data. *Ecological Modelling*, 143(3):227–243.
- Yang, K. and Koike, T. (2005). A general model to estimate hourly and daily solar radiation for hydrological studies. *Water resources research*, 41(10).

Appendix A

Appendix

Table A.1: Table showing A-P model constants proposed by Allen et al. (1998) and Anane (1986).

ALLEN ET AL.		
Region	a	b
Global	0.25	0.50
ANANE-FENIN		
Coastal south	0.267	0.463
Central region	0.247	0.420
Northern region	0.290	0.440

Table A.2: Estimated Monthly mean Clearness Index over the Savanna Zone.

Station	Clearness Index
Wa	0.66 – 0.47
Navrongo	0.67 – 0.50
Bole	0.63 – 0.42
Temale	0.64 – 0.48
Yendi	0.65 – 0.49

Table A.3: Estimated Monthly mean Clearness Index over the Transition Zone.

Station	Clearness Index
Wench	0.60 – 0.40
Sunyani	0.57 – 0.38
Keta Krachi	0.64 – 0.46

Table A.4: Estimated Monthly mean Clearness Index over the Forest Zone.

Station	Clearness Index
Kumasi	0.56 – 0.37
Sefwi Bekwai	0.58 – 0.36
Oda	0.56 – 0.39
Abetifi	0.61 – 0.45
Koforidua	0.60 – 0.39
Ho	0.61 – 0.41
Akuse	0.57 – 0.42
Akatsi	0.58 – 0.25

Table A.5: Estimated Monthly mean Clearness Index over the Coastal Zone.

Station	Clearness Index
Axim	0.58 – 0.35
Takoradi	0.60 – 0.38
Salt Pond	0.62 – 0.45
Accra	0.61 – 0.45
Tema	0.61 – 0.44
Ada	0.62 – 0.47

Table A.6: Statistical tests for Model Estimation over Savanna zone.

Station	RMSE	MBE	RMD	AMPE	r	t
Wa	4.9514	4.4776	0.2182	29.4981	0.1271	7.0266
Navrongo	4.5723	4.1816	0.2015	26.4225	0.2195	7.4990
Bole	3.9447	3.0747	0.1581	19.8845	-0.0418	4.12649
Temale	3.9524	3.4779	0.1730	21.8311	0.2746	6.1433
Yendi	4.4396	3.9673	0.1958	25.3864	0.1688	6.6032

Table A.7: Statistical tests for Model Estimation over Transition zone.

Station	RMSE	MBE	RMD	AMPE	r	t
Wenchi	3.9450	3.4599	0.1868	23.8809	0.3443	6.0546
Sunyani	2.8061	1.8535	0.1054	12.4201	-0.0114	2.9178
Kete Krachi	3.5801	2.8509	0.1453	18.0658	0.1749	4.3663

Table A.8: Statistical tests for Model Estimation over Forest zone.

Station	RMSE	MBE	RMD	AMPE	r	t
Kumasi	2.6467	1.5223	0.0864	9.9259	0.3618	2.3319
Sefwi Bekwai	2.0188	0.7532	0.0434	4.6390	0.5604	1.3338
Oda	2.0719	1.3828	0.0808	8.9545	0.5240	2.9725
Abetifi	4.2472	3.7174	0.1920	24.8438	0.1035	6.0023
Koforidua	2.4908	0.9202	0.0507	6.0513	0.2239	1.3186
Ho	2.9589	1.9684	0.1052	12.3510	0.2085	2.9550
Akuse	1.9671	0.5319	0.0302	3.5160	0.2582	0.9315
Akatsi	2.9397	0.6535	0.0371	4.1004	0.3616	0.7562

Table A.9: Statistical tests for Model Estimation over Coastal zone.

Station	RMSE	MBE	RMD	AMPE	r	t
Axim	2.1904	0.5291	0.0301	3.9187	0.6589	0.8256
Takoradi	2.6738	0.4612	0.0258	3.3782	0.3197	0.5808
Saltpond	3.5519	3.1079	0.1631	20.3278	0.6531	5.9942
Accra	2.3408	1.1440	0.0597	6.9515	0.4255	1.8580
Tema	2.0480	0.7287	0.0379	4.5003	0.4310	1.2628
Ada	2.1210	1.4409	0.0728	8.4121	0.6669	3.0705

Appendix B

Appendix

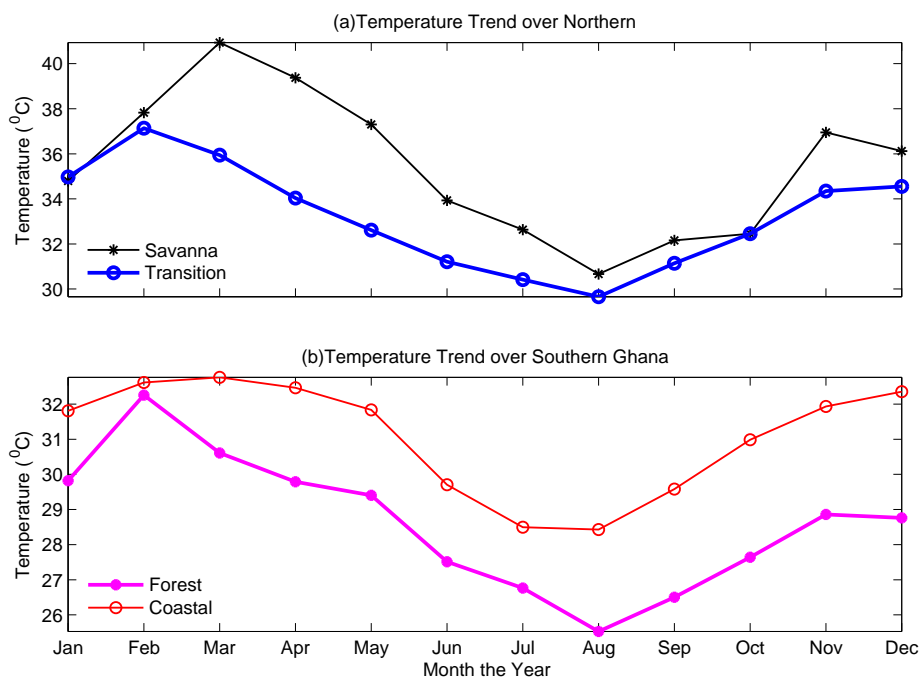


Figure B.1: Annual Monthly Mean Temperature Trend over the Four Agro-ecological zones of Ghana.

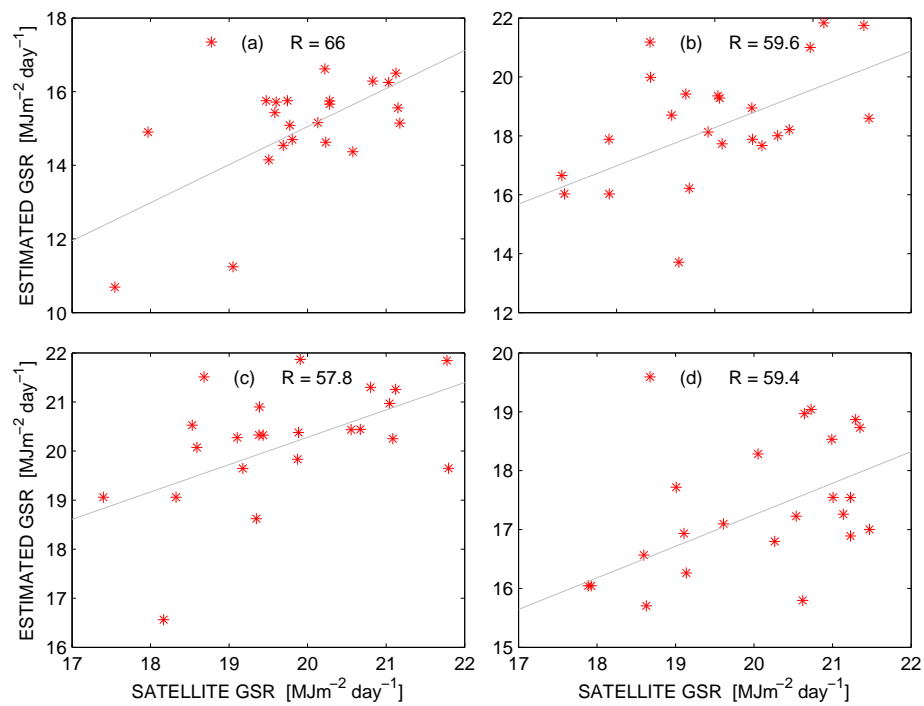


Figure B.2: Scatter plots comparing the linear correlation regression between estimated and satellite datasets of Global Solar radiation (GSR) for four selected months over the study area.

(a) represents June, (b) represents September, (c) October, and (d) represents November.

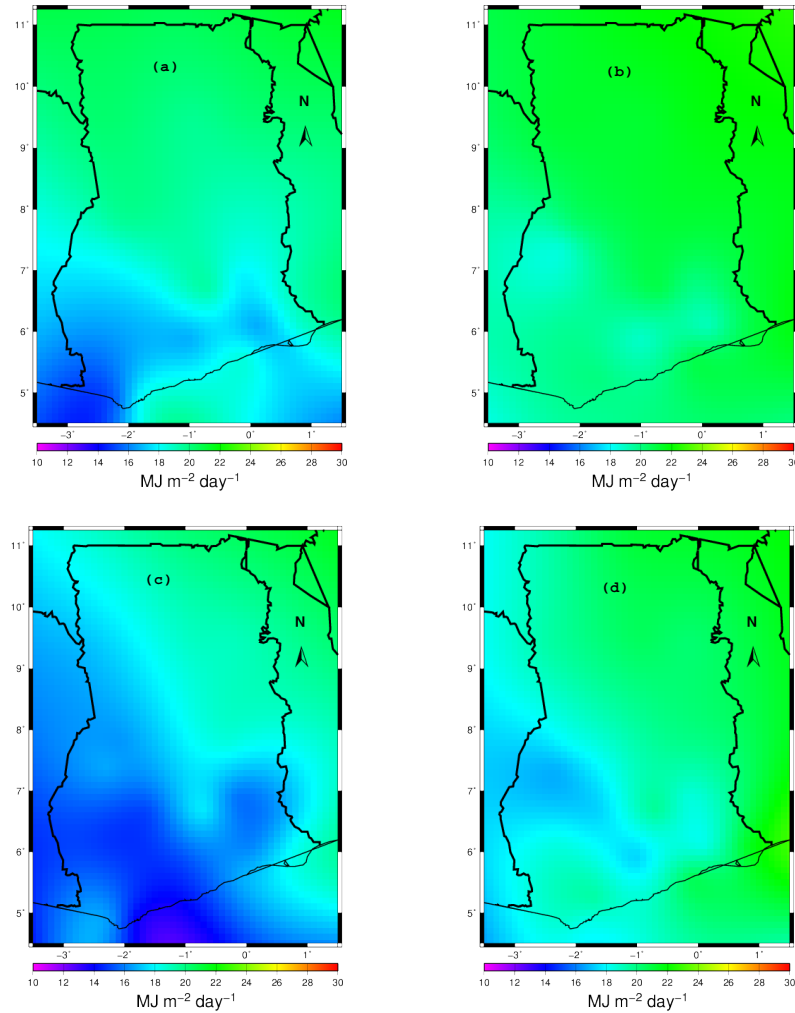


Figure B.3: Gridded Seasonal Global Solar Radiation estimate: (a) represents December-January-February (DJF), (b) represents March-April-May (MAM), (c) represents June-July-August (JJA) and (d) represents September-October-November (SON). The second trimester (MAM) showed the period with the highest Global Solar Radiation ($18.89\text{--}21.74 \text{ MJm}^{-2}\text{day}^{-1}$) levels over the study area, and the third trimester (JJA) showed the period with the lowest levels of Global Solar Radiation ($13.76\text{--}19.81 \text{ MJm}^{-2}\text{day}^{-1}$) for the study area.